

Developing dialkylammonium halide salts for industrial heat recovery at medium temperatures

Autora: Mar Jiménez Ávila

Tutor: Roc Matheu

Curs acadèmic: 2024–2025

Màster en Energies Renovables i Sostenibilitat Energètica







Developing dialkylammonium halide salts for industrial heat recovery at medium temperatures



Para empezar, quería expresar mi sincero agradecimiento al Dr. Roc Matheu, por su dedicación, su paciencia y sobre todo por su implicación incansable. Gracias por contar conmigo para formar parte del grupo *Matheulab*. Esta experiencia me ha permitido aprender, disfrutar, y conocer personas maravillosas, como lo son mis compañeros y amigos; Gerardo, Laura, Carlota, Xavi, Bea y Pau. Por otro lado, quiero expresar mi agradecimiento a los miembros del *Group of Characterization of Materials (GCM)*, especialmente al Dr. Pol Lloveras i el Dr. Josep Lluís Tamarit, por su ayuda durante la realización de este proyecto, y por su colaboración, permitiendo hacerlo posible.

Especialmente, quería agradecer a mis padres, María del Carmen y Alberto, por su apoyo continuo y su paciencia conmigo, os estoy muy agradecida por darme la oportunidad de vivir esta nueva aventura aquí, en Barcelona, y estar siempre para mí. Os quiero.

También deseo agradecerle a mi familia, especialmente a mis yayas Angelines y María, su apoyo y su enorme cariño.

Además, quiero darle las gracias a una persona especial, por motivarme en todo momento y estar ahí siempre que lo he necesitado, por ser tan paciente y hacerlo tan fácil. Samuel, gracias.

Gracias Kai, Katalina y Luna.





ABSTRACT

Today, continued population growth is leading to ever-increasing energy demand, which is driving the use of fossil fuels in today's energy consumption system. However, this entails a series of potentially harmful environmental impacts, among which global warming and the anthropogenic greenhouse effect stand out. Therefore, it is imperative to create sustainable solutions that will mitigate the consumption of fossil fuels and replace them with more efficient and environmentally friendly technologies.

One of the main challenges of the current energy system is to reduce the amount of thermal energy losses generated daily, especially in the industrial sector, which is responsible for a significant part of these losses. It is estimated that approximately 70% of the world's primary energy is dissipated in the form of waste heat, which has adverse environmental effects and also produces considerable economic losses due to the absence of efficient energy recovery and storage systems.

Throughout this project, we report the synthesis of *new* dialkylammonium halide salt compounds, whose general structure can be expressed as $(C_nH_{2n+1})_2NH_2X$, with different chain lengths (n = 10, 14, 16) and two types of halide anions (X = Cl, Br). They were characterized by powder X-ray diffraction (PXRD) and differential scanning calorimetry (DSC). The results show an evident correlation between chain length and lattice parameters, as well as improved transition temperature and enthalpy properties for the bromide salts, which are fundamental for industrial thermal storage applications. Some synthesized materials, like $(C_{16})_2Cl$, obtained promising technical results, exhibiting outstanding thermal behavior.

This investigation aims to illustrate the potential of novel and emerging materials, such as dialkylammonium halide salts, which have exhibited the desirable sustainable and efficient characteristics to aid in the energy transition.

Key words: transition temperature, latent heat, enthalpy, energy transition, phase change materials, industrial heat recovery, thermal energy storage, dialkylammonium halide salts.





RESUMEN

En la actualidad, el continuo crecimiento de la población supone una demanda energética cada vez mayor, que impulsa el uso de combustibles fósiles en el actual sistema de consumo energético. Sin embargo, esto conlleva una serie de impactos ambientales potencialmente dañinos, entre los que destacan el calentamiento global y el efecto invernadero antropogénico. Por lo tanto, es imperativo crear soluciones sostenibles que mitiguen el consumo de combustibles fósiles y los sustituyan por tecnologías más eficientes y respetuosas con el medio ambiente.

Uno de los principales retos del sistema energético actual es reducir las pérdidas de energía térmica que se generan a diario, especialmente en el sector industrial, responsable de una parte importante de estas pérdidas. Se calcula que aproximadamente el 70% de la energía primaria mundial se disipa en forma de calor residual, lo que provoca efectos adversos para el medio ambiente y produce considerables pérdidas económicas debido a la ausencia de sistemas eficientes de recuperación y almacenamiento de energía.

A lo largo de este proyecto, se reporta la síntesis de nuevos compuestos de sales de haluro de dialquilamonio, cuya estructura general puede expresarse como $(C_nH_{2n+1})_2NH_2X$, con diferentes longitudes de cadena (n=10, 14, 16) y dos tipos de aniones haluro (X=Cl, Br). Estos compuestos han sido caracterizaros mediante difracción de rayos X en polvo (PXRD) y calorimetría diferencial de barrido (DSC). Los resultados muestran una correlación evidente entre la longitud de cadena y los parámetros de red, así como una mejora en las propiedades relacionadas con la temperatura de transición y la entalpía de las sales de bromuro, que son fundamentales para aplicaciones industriales de almacenamiento térmico. Algunos materiales sintetizados, como $(C_{16})_2Cl$, obtuvieron resultados técnicos prometedores, demostrando un comportamiento térmico excepcional.

El propósito de esta investigación es demostrar el potencial de materiales novedosos y emergentes, como las sales de haluro de dialquilamonio, que han evidenciado características altamente sostenibles y eficientes, adecuadas para contribuir con la transición energética.

Palabras clave: temperatura de transición, calor latente, entalpía, transición energética, materiales de cambio de fase, recuperación de calor industrial, almacenamiento de energía térmica, sales de haluro de dialquilamonio.







RESUM

En l'actualitat, el continu creixement de la població implica una demanda energètica cada vegada major, que impulsa l'ús de combustibles fòssils en l'actual sistema de consum energètic. Tanmateix, això comporta una sèrie d'impactes ambientals potencialment nocius, entre els quals destaquen l'escalfament global i l'efecte d'hivernacle antropogènic. Per tant, és imperatiu crear solucions sostenibles que mitiguin el consum de combustibles fòssils i els substitueixin per tecnologies més eficients i respectuoses amb el medi ambient.

Un dels principals reptes del sistema energètic actual és reduir les pèrdues d'energia tèrmica que es generen diàriament, en especial, al sector industrial, responsable d'una part important d'aquestes pèrdues. Es calcula que, aproximadament el 70% de l'energia primària mundial es dissipa en forma de calor residual, la qual cosa provoca efectes adversos per al medi ambient i produeix considerables pèrdues econòmiques a causa de l'absència de sistemes eficients de recuperació i emmagatzematge d'energia.

Al llarg d'aquest projecte, es reporta la síntesi de nous compostos de sals d'halur de dialquilamoni, l'estructura general dels quals pot expressar-se com $(C_nH_{2n+1})_2NH_2X$, amb diferents longituds de cadena (n=10, 14,16) i dos tipus d'anions halur (X=Cl, Br). Aquests compostos es van caracteritzar mitjançant difracció de raigs X en pols (PXRD) i calorimetria diferencial d'escombratge (DSC). Els resultats mostren una correlació evident entre la longitud de cadena i els paràmetres reticulars, així com una millora de la temperatura de transició i de les propietats d'entalpia de les sals de bromur, fonamentals per a aplicacions d'emmagatzematge tèrmic industrial. Alguns materials sintetitzats, com $(C_{16})_2Cl$, van obtenir resultats tècnics prometedors, demostrant un comportament tèrmic excepcional.

El propòsit d'aquesta recerca és demostrar el potencial de materials nous i emergents, com les sals d'halur de dialquilamoni, que han evidenciat característiques altament sostenibles i eficients, adequades per a contribuir amb la transició energètica.

Paraules clau: temperatura de transició, calor latent, entalpia, transició energètica, materials de canvi de fase, recuperació de calor industrial, emmagatzematge d'energia tèrmica, sals d'halur de dialquilamoni.





SUSTAINABLE DEVELOPMENT GOALS (SDGs)

This Master's Thesis aims to address the context of sustainability by contributing directly to some of the current Sustainable Development Goals (SDGs), defined by the United Nations Agenda 2030.



First, the project falls within **SDG 9**, which refers to *Industry*, *Innovation*, *and Infrastructure*, as it focuses on the innovation of new materials, such as phase-change materials (PCMs), to transform the current energy system, reducing energy losses and promoting sustainable industrialization. This project contributes to materials research applied to industry and infrastructure, paving the way for innovation.



On the other hand, it also contributes to **SDG 7**: Affordable and Clean Energy by exploring phase-change materials capable of sustainably storing and releasing thermal energy. The goal is to improve the efficiency of thermal energy storage in both industry and residential sectors, reducing energy consumption and, consequently, greenhouse gas emissions. Furthermore, its integration with renewable energy sources contributes to the decarbonization of the industrial sector, achieving a cleaner energy system.



In addition, this project is well aligned with **SDG 12**, which refers to **Responsible Production and Consumption**, as it contributes to a more efficient management of energy resources. The objective is to minimize losses and promote the rational use of energy through the incorporation of new technologies. This approach would make it possible to reduce the demand for resources and the environmental impact while promoting more responsible energy production.





TABLE OF CONTENTS

ABSTRACT	1
RESUMEN	2
RESUM	3
SUSTAINABLE DEVELOPMENT GOALS (SDGs)	4
INDEX OF TABLES	7
INDEX OF FIGURES	8
1. INTRODUCTION	10
1.1. ENERGY LOSSES AND THERMAL STORAGE	10
1.2. OVERVIEW OF SOLID-SOLID PHASE CHANGE MATERIALS (SS-PCMs)	11
1.3. HYBRID MATERIALS FOR THERMAL STORAGE	12
1.4. DIALKYLAMMONIUM HALIDE SALTS AS EMERGING SS-PCMs	13
2. OBJECTIVES	17
3. RESULTS AND DISCUSSION	18
3.1. SYNTHESIS OF NEW DIALKYLAMMONIUM HALIDE SALTS AND STRUCTURAL CHARACTERIZATION	18
3.2. THERMODYNAMIC CHARACTERIZATION	21
3.3. INDUSTRIAL APPLICABILITY OF MATERIALS	24
3.3.1. HEAT PUMPS AND SANITARY HOT WATER	24
3.3.2. BAROCALORIC POTENTIAL	25
3.3.3. THERMAL CONTROL IN SUSTAINABLE BUILDING	26
3.3.4. SYNERGY WITH SOLAR RENEWABLE ENERGY	26
3.3.5. INTEGRATION OF SS-PCMs INTO BATTERY DESIGN	26
4. EXPERIMENTAL METHODS	27
4.1. MATERIALS	27
4.1.1. REAGENTS	27
4.1.2. SYNTHESIS OF $(C_n)_2Cl$	27
4.1.2.1. SYNTHESIS OF (C ₁₀ H ₂₁) ₂ NH ₂ Cl	27
4.1.2.2. SYNTHESIS OF (C ₁₄ H ₂₉) ₂ NH ₂ Cl	27
4.1.2.3. SYNTHESIS OF (C ₁₆ H ₃₃) ₂ NH ₂ Cl	27
4.1.3. SYNTHESIS OF $(C_n)_2$ Br	28
4.1.3.1. SYNTHESIS OF (C ₁₀ H ₂₁) ₂ NH ₂ Br	28
4 1 3 2 SYNTHESIS OF (C14H20)2NH3Rr	28



Developing dialkylammonium halide salts for industrial heat recovery at medium temperatures



4.1.3.3. SYNTHESIS OF $(C_{16}H_{33})_2NH_2Br$	28
4.2. METHODS	28
4.2.1. POWDER X-RAY DIFFRACTION (PXRD)	28
4.2.2. BALL MILLING	29
4.2.3. DIFFERENTIAL SCANNING CALORIMETRY (DSC)	29
5. CONCLUSIONS	30
6. REFERENCES	31
7. ACRONYMS	34
APPENDICES	35
APPENDIX I. PXRD DATA	36
APPENDIX II. DSC DATA	37







INDEX OF TABLES

Table 1. Results of the lattice parameter a, b, c (Å) for each simulated and experi	mental sample
$(\lambda = 1.54054 \text{ Å})$	36
Table 2. Numerical results of transition temperature and latent heat values extract	ted by DSC for
each synthesized powder	37





INDEX OF FIGURES

Figure 1. Scheme of a thermal energy storage system
Figure 2. Specific examples of each category of solid-solid phase change materials. $[C(CH_2OH)_4], [(C_{10}H_{21}NH_3)_2MnCl_3], $ and $[(Ni_{41}Mn_{31}Ti13)_{41}B_2]$ respectively
Figure 3. Single-crystal structure of $(C_{10}H_{21}NH_3)_2CuCl_4$
Figure 4. Transition temperature (T_T) behavior of dialkylammonium chlorine perovskites as a function of the number of carbon atoms in the chain (n)
Figure 5. Latent heat (ΔH) behavior of dialkylammonium chlorine perovskites as a function of the number of carbon atoms in the chain (n)
Figure 6. Representation of how dialkylammonium halide salts pattern the arrangement of hydrocarbon bilayers in a manner analogous to that of 2D metal halide perovskites. $X = Cl$, Br
Figure 7. Transition temperature (T_T) and latent heat (ΔH) behavior of $(C_n)_2Cl$ as a function of the number of carbon atoms in the chain (n)
Figure 8. Transition temperature (T_T) and latent heat (ΔH) behavior of $(C_n)_2Br$ as a function of the number of carbon atoms in the chain (n)
Figure 9. Synthesis of dialkylammonium halide salts from dialkylamines ($n = 10, 14, 16$) and hydrohalic acid ($X = Cl, Br$)
Figure 10. PXRD patterns for $(C_n)_2Cl$ $(n = 10, 14, 16)$
Figure 11. PXRD patterns for $(C_n)_2Br$ $(n = 10, 14, 16)$
Figure 12. Growth of lattice parameter (b) with respect to the number of carbons in the chain (n)
Figure 13. DSC results for $(C_{14})_2Cl$ and $(C_{16})_2Cl$
Figure 14. Comparative DSC thermograms of dialkylammonium halide salts with a single reversible transition for each compound (Cl, Br)
Figure 15. Transition temperature (T_T) and latent heat (ΔH) of $(C_n)_2Cl$ synthesized in the current project $(n = 10, 14, 16)$ graphically compared with those already known $(n = 6, 8, 10, 12)$
Figure 16. Transition temperature (T_T) and latent heat (ΔH) of $(C_n)_2Br$ synthesized in the current project $(n = 10, 14, 16)$ graphically compared with those already known $(n = 6, 10, 12, 18,, 24)$



Developing dialkylammonium halide salts for industrial heat recovery at medium temperatures



Figure 17. Diagram of a heat pump incorporating a TES system with diag	lkylammonium halide
salts	25
Figure 18. DSC results for $(C_{10})_2Cl$	38
Figure 19. DSC results for $(C_{10})_2Br$	38
Figure 20. DSC results for $(C_{14})_2Cl$	39
Figure 21. DSC results for $(C_{14})_2Br$	39
Figure 22. DSC results for (C ₁₆) ₂ Cl	40
Figure 23 DSC results for (C ₁₆) ₂ Br	40





1. Introduction

1.1. ENERGY LOSSES AND THERMAL STORAGE

Industry is one of the most energy-intensive sectors worldwide and, at the same time, one of the main contributors to thermal energy loss during its processes. Approximately 72 % [1] of the world's primary energy consumption is estimated to be wasted as residual heat. More specifically, 19 % [1] is a consequence of the industrial sector, mainly due to equipment such as furnaces [2], natural gas boilers, and turbines. This vast amount of unused energy represents a key opportunity for industrial heat recovery, a highly promising strategy that can significantly enhance energy efficiency in most of today's industrial processes. The implementation of thermal energy storage (TES) technologies [3] would enable the capture and storage of waste heat, allowing it to be reused in other processes that require it, reducing the current dependence on fossil fuels and contributing to a circular economy [2]. This system [4], [5] generally works as shown in Figure 1.

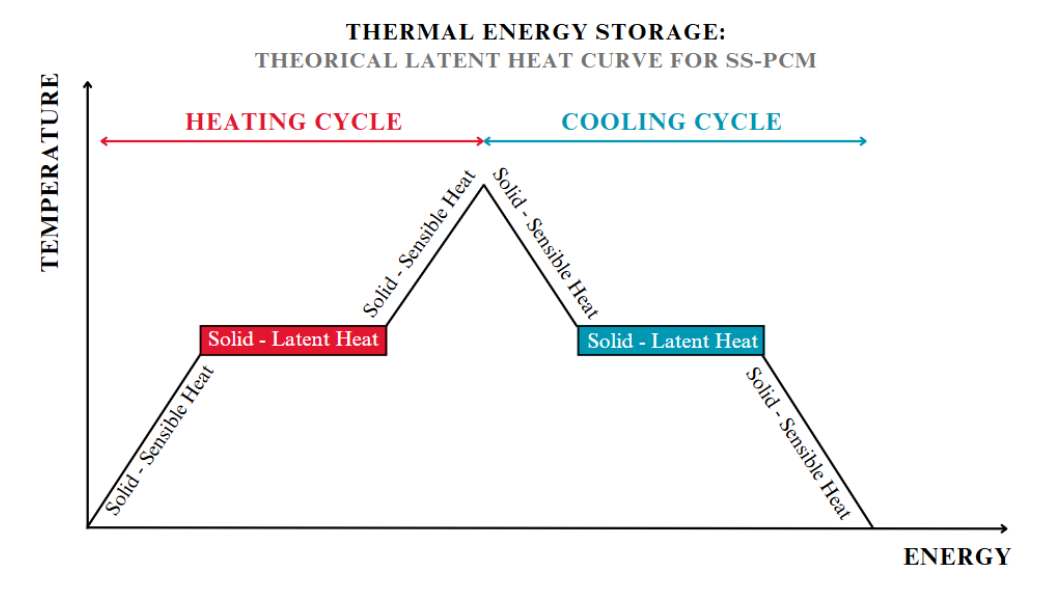


Figure 1. Scheme of a thermal energy storage system.

Regarding this field, one of the most attractive approaches to TES is the use of phase change materials (PCMs) ^[6], which can efficiently store and release thermal energy through phase transitions. TES can be categorized into three mechanisms ^[7]: sensible heat storage, latent heat storage, or thermochemical storage. This project focuses on latent heat storage, which leverages the phase change of specific materials to efficiently absorb and release heat through a reversible phase transition at a given temperature.

Equation (1) defines the latent heat storage process, quantifying the thermal energy stored or released. In this case, it is a solid-solid transition, where the crystalline lattice of the material is restructured isothermally, without changing to a gas or liquid state, remaining solid. The total heat exchanged (ΔQ) is directly proportional to the mass of material (m) and the latent heat of the transition (ΔH).

$$\Delta Q = m \cdot \Delta H \tag{1}$$





1.2. OVERVIEW OF SOLID-SOLID PHASE CHANGE MATERIALS (SS-PCMs)

Solid-solid phase change materials (SS-PCMs) are particularly attractive due to their significant advantages [3] over solid-liquid phase change materials (SL-PCMs). Some of these advantages are the compactness of the material, in line with the reduced possibility of leakage [3], as they maintain their solid structure during exchange, undergoing a structural transition [2] in their crystal lattice at a specific temperature depending on their composition and application. The latent heat storage capacity of SS-PCMs is determined by the difference in degrees of freedom between the ordered and disordered phases [8], [9], while the phase transition temperature depends on the strength of the non-covalent interactions between molecules. Within PCMs, there are different classes that are currently under scientific research due to their great potential for many applications. SS-PCMs are divided into three broad categories: organic, inorganic, and hybrid (Figure 2).

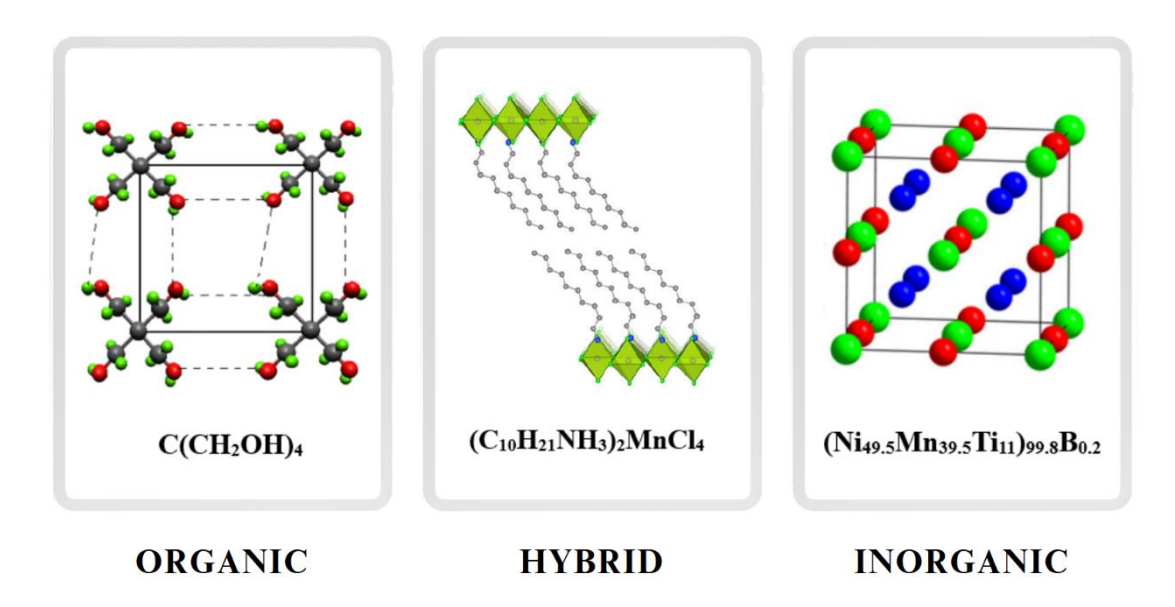


Figure 2. Specific examples of each category of solid-solid phase change materials. [C(CH₂OH)₄], [(C₁₀H₂₁NH₃)₂MnCl₃], and [(Ni₄₁Mn₃₁Ti13)₄₁B₂] respectively. [10], [11], [12].

Organic crystalline molecules ^[7] exhibit energetic S-S phase transitions from their crystalline structure to a different crystalline configuration with high polymorphic flexibility. These materials crystallize through intermolecular interactions such as hydrogen bonds ^[13], forming compact structures that determine their thermal stability. Their packing influences thermal conductivity and energy storage capacity, providing advantageous properties for industrial heat storage. The more ordered the structure, the better the long-term stability ^[13], but with the risk of limiting heat transfer. This family consists of polyalcohols ^[14], plastic crystals, polymeric materials, and others based on organic salts. Their latent heat typically ranges from 15 to 270 kJ·kg⁻¹ ^[7], with transition temperatures between 25 and 185 °C ^[7].

On the other hand, inorganic SS-PCMs, which can be ceramic or metallic materials, are those capable of reversibly storing and releasing thermal energy through the order-disorder transition facilitated by magnetic and crystallographic structure transformation. They usually have high latent heat storage, melting point, and thermal conductivity. Their transition temperature range is between 30 and 120 $^{\circ}$ C $^{[7]}$, with latent heat values between 25 and 70 kJ·kg $^{-1}$ $^{[7]}$, which are lower







than those of organic materials. Examples of inorganic SS-PCMs are inorganic salts ^[15], such as lithium sulfate (Li₂SO₄), which changes its crystalline structure as a function of temperature, or transition metal oxides ^{[16], [17]}, such as vanadium oxide (VO₂), which exhibits a reversible metal-to-insulator phase transition (MIT).

1.3. HYBRID MATERIALS FOR THERMAL STORAGE

Finally, hybrid SS-PCMs have attracted considerable interest due to their high thermal stability ^[7], although they generally have a slightly lower latent heat than other conventional SS-PCMs. Hybrid materials consist of organic and inorganic sublattices ^[2] that can be designed independently, such as perovskites and organometallic compounds. These materials comprise structures that include an inorganic sublattice (such as a network of metal halides) and an organic sublattice ^[7] formed by organic cations. Interaction between the two sublattices ^[18] occur through ionic bonds and intermolecular van der Waals forces ^[2], allowing the organic cations to undergo solid-solid phase transitions. Their thermal storage mechanism is based on the pseudomelting of these crystalline sections by absorbing thermal energy, and the subsequent heat release during the cooling process, which is a completely reversible cycle.

In hybrid materials, phase transitions are strongly dependent on entropy changes [19], which are based on the difference in degrees of freedom (G) between the phases. Therefore, it is essential to search for structures that can exhibit solid-solid transitions involving distortions with significant changes in the degrees of freedom. As mentioned above, it is possible to optimize these materials' organic and inorganic sublattices separately to reach the desired requirements. These customizations of physical and thermal properties have resulted in materials with highly flexible behavior due to their perfect crystalline structure, which is configured to work at medium-high temperatures.

This project focuses on the development of hybrid SS-PCMs. To do so, we must first introduce perovskites. Perovskites have been widely investigated due to their remarkable properties in light-absorbing and light-emitting applications [20], [21]. In those applications, perovskites typically have a 3D structure of the general formula ABX_3 [22]. In this structure, small monovalent A-site cations are located in the holes formed by a lattice of BX_6 octahedra connected at the corners, where B is a divalent metal, and X is a halide ion (Cl, Br, I).

Related to their 3D congeners, 2D perovskites are emerging PCMs. The dimensional reduction can be understood as a formal addition of an AX salt to 3D perovskites, leading to 2D perovskites (ABX₃+ AX = A_2BX_4). In 2D perovskites, layers of BX₆ octahedra are stacked and separated by larger organic A-site cations, forming a layered structure (Figure 3). This arrangement increases the compositional versatility of 2D perovskites, which now can incorporate large alkylammonium cations (Figure 3), opening the room to be used in applications beyond light-absorbing and light-emitting applications.





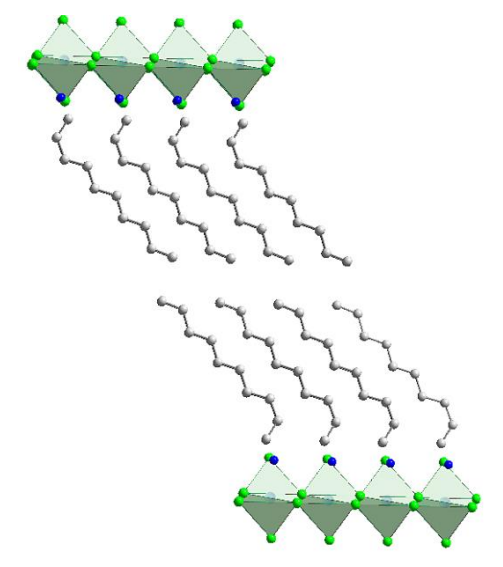


Figure 3. Single-crystal structure of $(C_{10}H_{21}NH_3)_2CuCl_4$ [3], [23].

1.4. DIALKYLAMMONIUM HALIDE SALTS AS EMERGING SS-PCMs

Alkylammonium perovskites have been studied by the *Matheulab* group at the *University of Barcelona (UB)*. Below, their results are compared with bibliographic data ^[24]. The group previously synthesized a series of 2D alkylammonium perovskites $(C_nH_{2n+1}NH_3)_2CuCl_4$ with an increasing number of carbons in the alkylammonium chain (n). Previous work focused on materials with longer n (16–22) with respect to previous compounds (n < 17). Figure 4 shows the transition temperatures $(C_nH_{2n+1}NH_3)_2CuCl_4$ with respect to the atom number n of the alkylammonium cations for $(C_nH_{2n+1}NH_3)_2CuCl_4$. For n > 20, the new perovskites show favorable transition temperatures for industrial applications, some above 100 °C. On the other hand, Figure 5 shows the latent heat associated with the transition as a function of n. Here, we can observe that a latent heat decrease is observed for $(C_nH_{2n+1}NH_3)_2CuCl_4$ with n > 16.

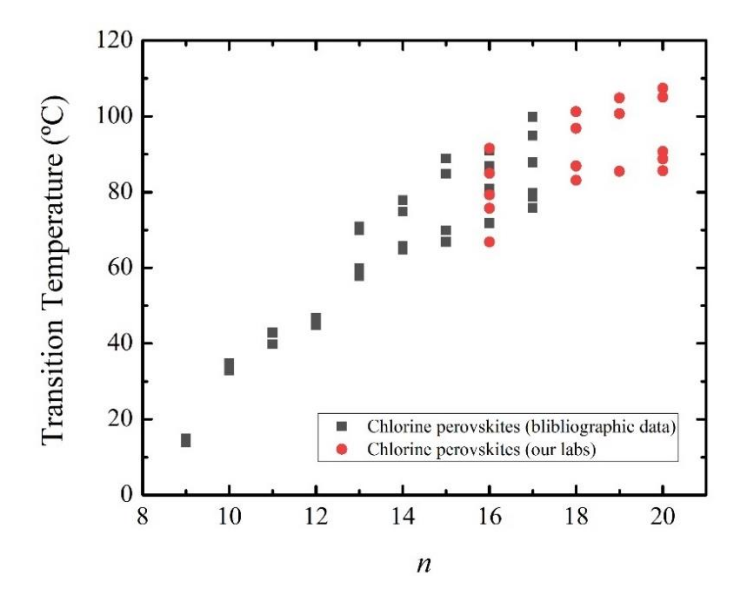


Figure 4. Transition temperature (T_T) behavior of dialkylammonium chlorine perovskites as a function of the number of carbon atoms in the chain $(n)^{[18], [24], [25]}$.





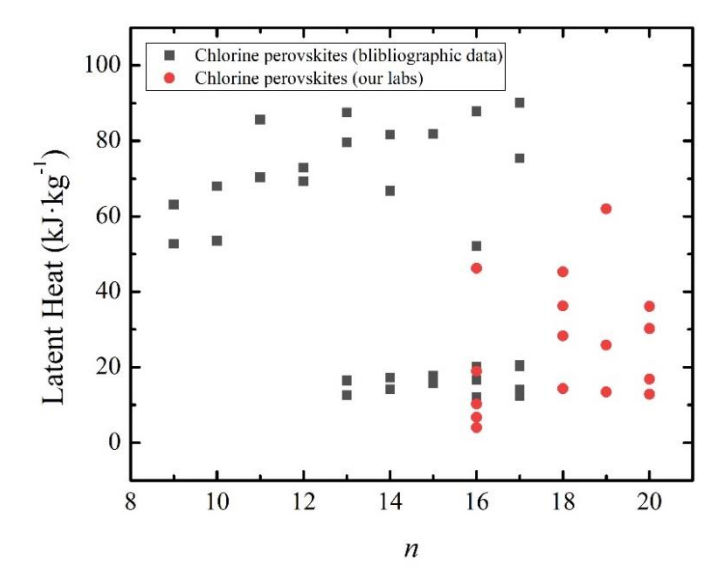


Figure 5. Latent heat (ΔH) behavior of dialkylammonium chlorine perovskites as a function of the number of carbon atoms in the chain $(n)^{[18],[24],[25]}$.

Although 2D perovskites reached high transition temperatures suitable for industrial applications, their latent heat values decreased with increasing alkyl chain length, limiting their energy storage capacity. This prompted the exploration of alternative materials with potentially higher transition enthalpies, such as dialkylammonium halide salts. These ionic compounds consist of organic cations (dialkylammonium) and halide anions (X) [25], which, unlike 2D perovskites, do not contain metal atoms (Figure 6). 2D perovskites are characterized by the alternation of inorganic octahedral layers (BX₆) with organic layers in a hybrid structure. In contrast, the crystal lattice of the salts is formed by the dialkylammonium ion, which consists of a positively charged ammonium group (R₂NH₂⁺) attached to two long alkyl chains. Although these salts lack extended inorganic layers, they exhibit lamellar packing of hydrocarbon chains and halide anions, showing an arrangement analogous to that found in 2D metal halide perovskites. The general formula of these salts is $(C_nH_{2n+1})_2NH_2X$ (X = Cl, Br), and the number of carbon atoms in the alkyl groups (n) is typically greater than 10, reflecting the common presence of long hydrocarbon chains in these compounds.

While dialkylammonium halide salts are formally organic materials, their behavior exhibits certain similarities to hybrid materials, especially regarding thermal stability and energy storage mechanisms [26]. As such, they represent a relatively new option as an energy storage material, with advantages such as high thermal and chemical stability, economic viability, and low vapor pressure, in addition to being an environmentally friendly alternative.





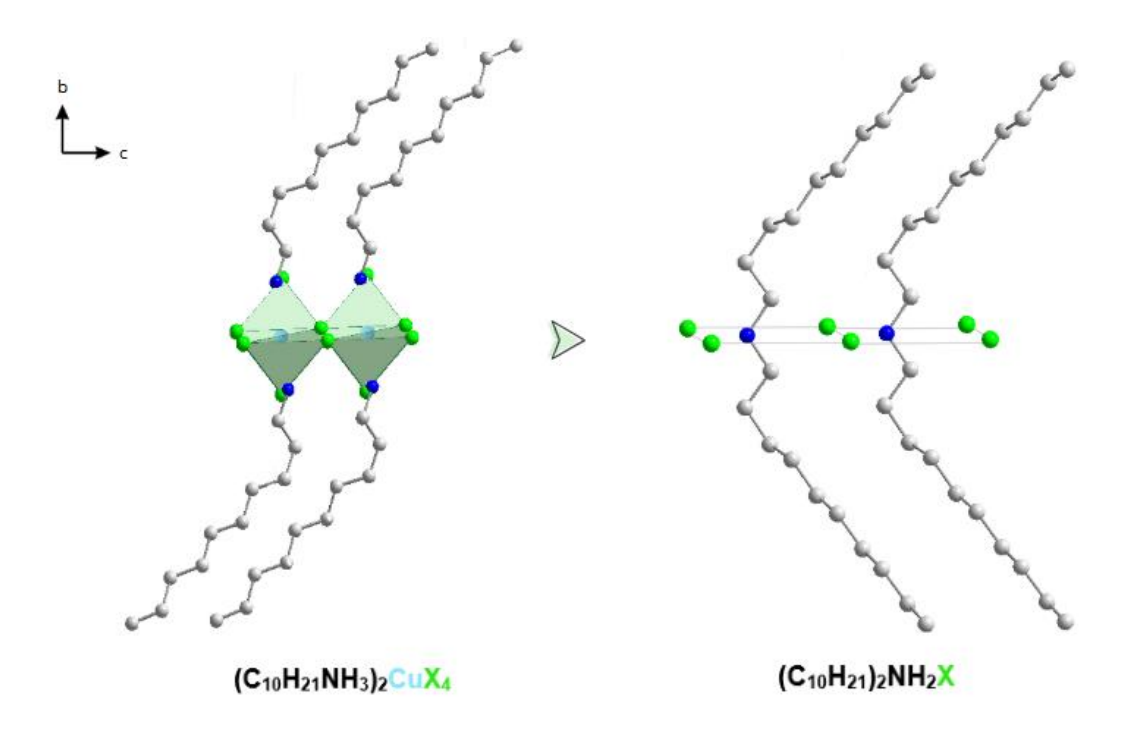


Figure 6. Representation of how dialkylammonium halide salts pattern the arrangement of hydrocarbon bilayers in a manner analogous to that of 2D metal halide perovskites. X = Cl, Br [25].

The available literature on the materials selected for development in this project (dialkylammonium halide salts) provides data on their transition temperature and latent heat, which are the main parameters considered in this study (Figure 7–8). Additional parameters will be needed to fully characterize these alternative materials for their application as PCMs, such as their response to pressure for potential barocaloric applications. Nevertheless, this project focuses on the transition temperature and the resulting latent heat, two of the most relevant parameters for initially comparing these systems with others.

Studies have primarily focused on compounds with shorter alkyl chain lengths (up to n = 12) for $(C_nH_{2n+1})_2NH_2X$ (X = Cl, Br). The transition temperatures for $(C_nH_{2n+1})_2NH_2X$ (X = Cl, Br) follow an upward trend with the number of carbon atoms in the alkyl chain (n) (Figure 7–8). Interestingly, and contrary to halide perovskites, the latent heat for $(C_nH_{2n+1})_2NH_2X$ (X = Cl, Br) (Figure 5) increases with n. Thus, in view of the information reported, it is believed that these salts may be very promising for thermal energy storage applications, acting as PCMs. Therefore, this project aims to synthesize these salts with longer alkyl chains in order to obtain the missing data and complete the sequence. The goal is to determine whether the favorable behavior observed thus far continues with increasing chain length or if it deteriorates and becomes no longer viable.





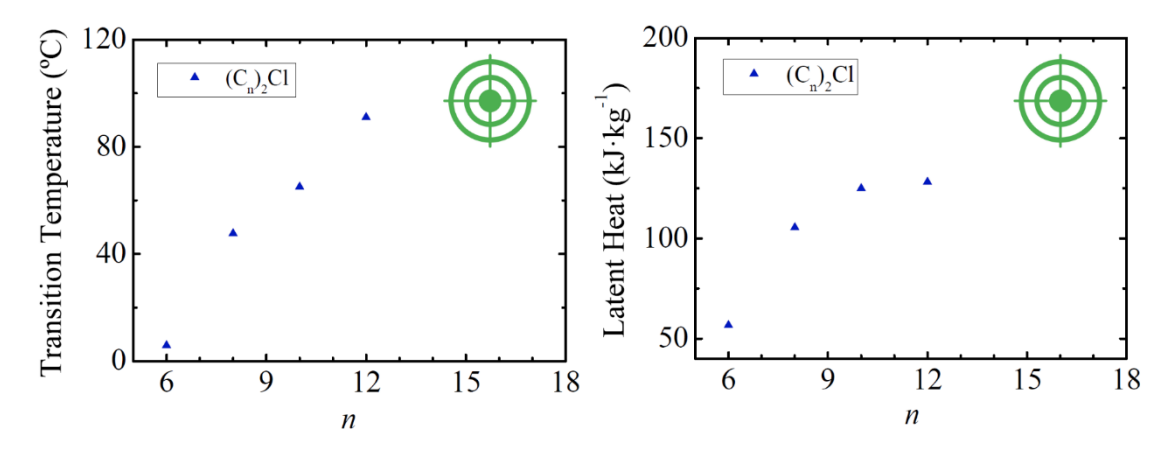


Figure 7. Transition temperature (T_T) and latent heat (ΔH) behavior of $(C_n)_2Cl$ as a function of the number of carbon atoms in the chain (n) [18], [24], [25].

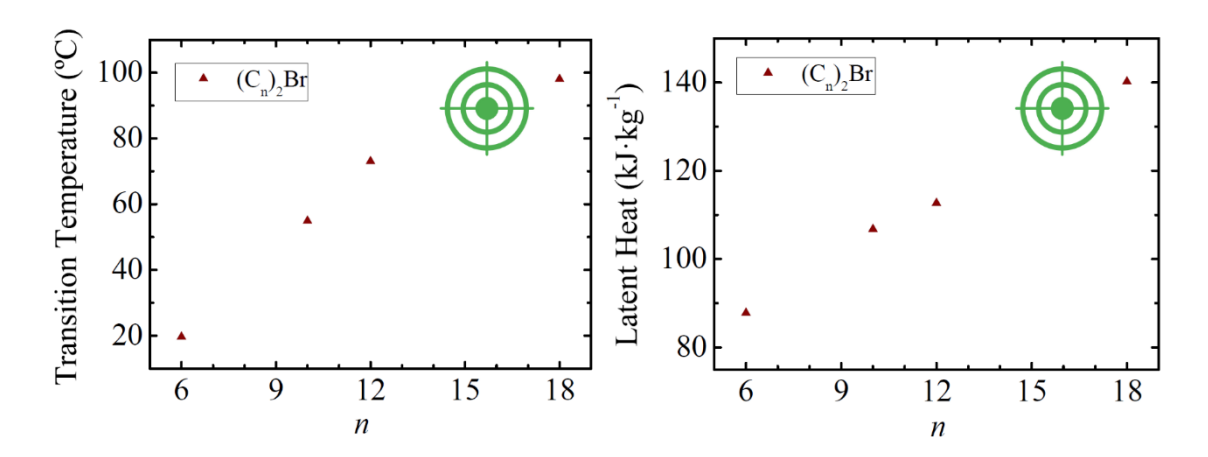


Figure 8. Transition temperature (T_T) and latent heat (ΔH) behavior of $(C_n)_2$ Br as a function of the number of carbon atoms in the chain $(n)^{[18],[24],[25]}$.





2. OBJECTIVES

This study aims to investigate the thermal properties and behavior of newly synthesized SS-PCMs for intermediate-temperature industrial energy storage applications. To achieve this, the project will analyze the thermal performance of *new* dialkylammonium salts, the relationship between their molecular structure and phase transition behavior, and their overall suitability for industrial implementation. Additionally, we will evaluate the associated challenges and limitations, as well as their potential for large-scale adoption based on the thermodynamic properties required for their intended applications. Thus, the specific objectives (**0**) of this project are:

- **O1.** To carry out the synthesis and structural characterization of previously unreported dialkylammonium halide salts with chain lengths n = 10, 14, and 16, whose final structure is $(C_nH_{2n+1})_2N^+H_2X^-$ (X = Br, Cl). X-ray diffraction measurements will be performed on the powder obtained to identify its reflections and observe the differences between the halides and carbon numbers.
- **O2.** To analyze, using DSC, the order-disorder transitions, their temperatures, and the entropy change produced. Once the results have been determined, they will be compared with previous studies for the same material but with shorter chain lengths.
- **O3.** To investigate future applications in the field of industrial energy recovery based on the data obtained.





3. RESULTS AND DISCUSSION

3.1. SYNTHESIS OF NEW DIALKYLAMMONIUM HALIDE SALTS AND STRUCTURAL CHARACTERIZATION

We started attempting the synthesis of $(C_n)_2Cl$ (n = 10, 14, and 16) (Figure 9). First, the di-n-alkylamine was dissolved in hexane, and then the second reagent, hydrochloric acid (HCl), was added to the solution. After two hours $(C_n)_2Cl$ (n = 10, 14, and 16) was obtained.

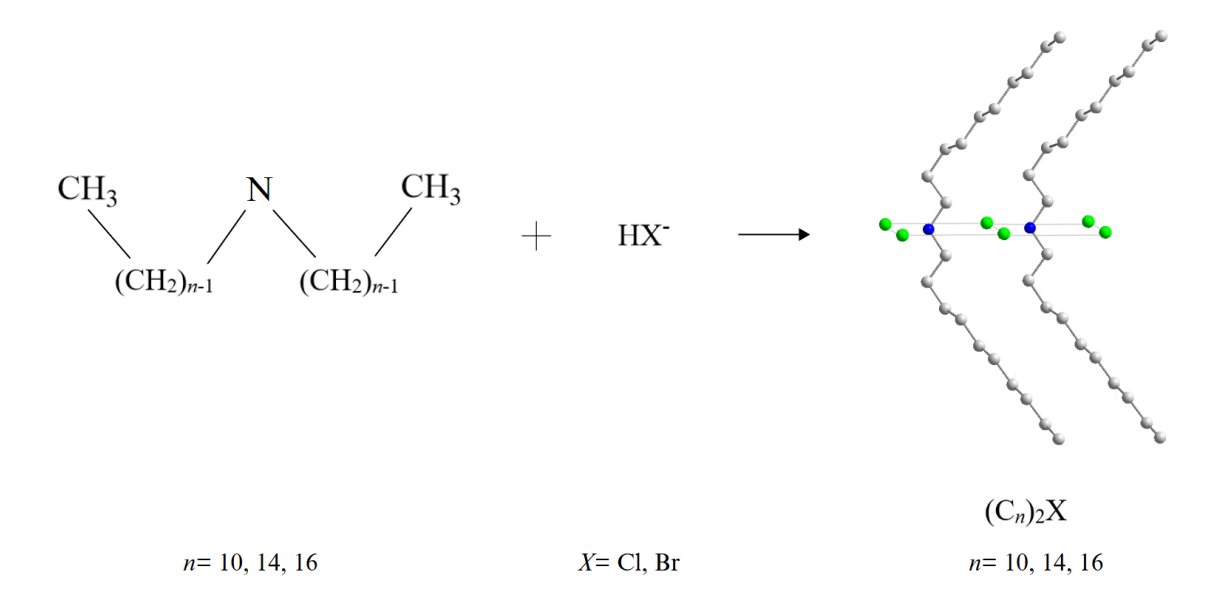


Figure 9. Synthesis of dialkylammonium halide salts from dialkylamines (n = 10, 14, 16) and hydrohalic acid (X = Cl, Br).

Powder X-ray diffraction was performed on $(C_{10})_2\text{Cl}$, $(C_{14})_2\text{Cl}$ and $(C_{16})_2\text{Cl}$. The samples were ground by ball milling to avoid preferential orientation. The PXRD pattern for $(C_{10})_2\text{Cl}$ shows at least seven intense reflections at 2θ (λ = 1.54054 Å) = 4.20 °, 12.51 °, 17.28 °, 20.96 °, 22.31 °, 23.56 ° and 24.72 ° (Figure 10). These diffractions match those simulated by SCXRD data ^[25] and correspond to the (0,2,0), (0,6,0), (0,2,1), (0,6,1), (0,7,1), (1,7,0) and (1,0,-1) planes (Figure 10). Then, we analyzed $(C_{14})_2\text{Cl}$ and $(C_{16})_2\text{Cl}$ by PXRD. The PXRD peaks related to the b axis (e.g., 0,2,0) clearly show a decrease of 2θ for $(C_{14})_2\text{Cl}$ (3.30 °) and $(C_{16})_2\text{Cl}$ (2.50 °) in comparison to $(C_{10})_2\text{Cl}$ (4.20 °), which is reflected by a shift of the peaks to the left. Contrary, the peaks related to the a and c axes remain unvaried with the increased n. This clearly indicates that the extended length of the chain mostly affects the b parameter, while leaving the a-c unchanged. We then calculate the lattice parameters (a, b, c) assuming an orthorhombic cell, and compare the signals of the experimental PXRD pattern with the simulated SCXRD pattern (Table 1).





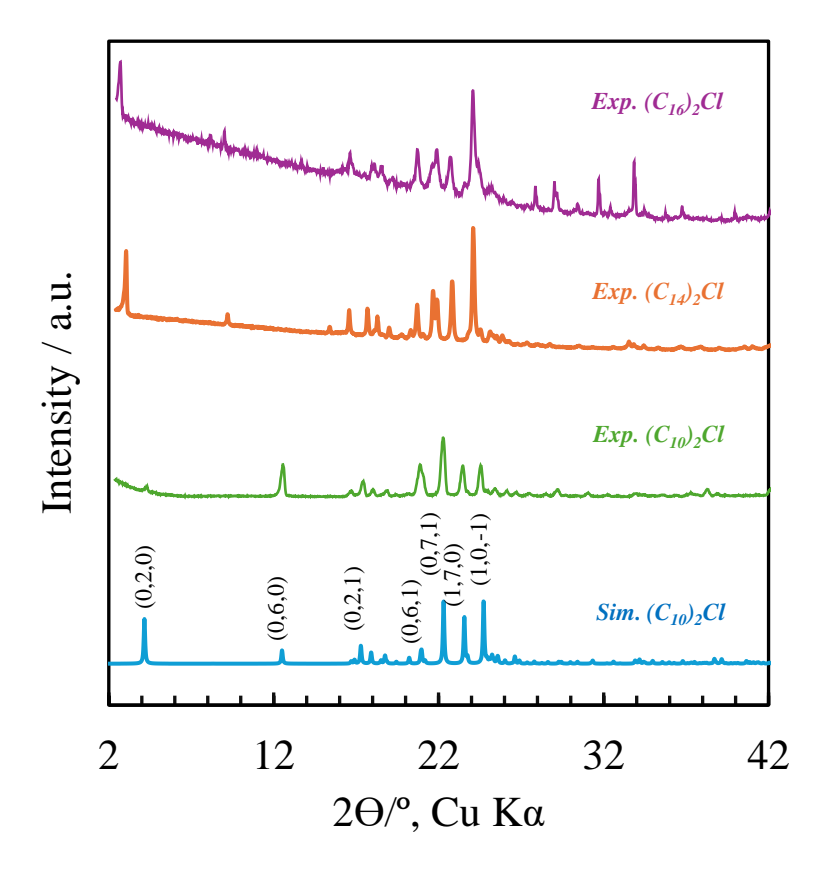


Figure 10. PXRD patterns for $(C_n)_2C1$ (n = 10, 14, 16).

After that, we prepared $(C_n)_2$ Br (n = 10, 14, and 16) by dissolving di-n-alkylamine in hexane and then adding hydrobromic acid (HBr) to the solution. Once the reaction was completed, $(C_n)_2$ Br (n = 10, 14 and 16) was obtained. The $(C_{10})_2$ Br, $(C_{14})_2$ Br, and $(C_{16})_2$ Br powders were ground by ball milling to avoid preferential orientation and subsequently analyzed by PXRD. The PXRD patterns for $(C_{10})_2$ Br show intense reflections at 2θ ($\lambda = 1.54054$ Å) = 4.43°, 8.87°, 13.32°, 19.32°, 22.96°, 23.67° and 24.09° (Figure 11), identical to the pattern simulated from SCXRD data $^{[25]}$, which corresponds to (0,2,0), (0,4,0), (0,6,0), (1,5,0), (0,7,1), (1,0,1) and (1,2,1) planes (Figure 11). Furthermore, we measured $(C_{14})_2$ Br and $(C_{16})_2$ Br by PXRD in conjunction with $(C_{10})_2$ Br. The PXRD peaks related to the b-axis (e.g., 0,6,0) evidence a decrease of 2θ (shifted to the left) for $(C_{14})_2$ Br (10.20°) and $(C_{16})_2$ Br (8.90°) compared to $(C_{10})_2$ Br (13.32°). Similarly, as for $(C_{10})_2$ Cl, the peaks associated with the a and c axes remain invariant as the number of carbons in the chain increases. This evidences that the chain length mainly affects the b parameter. The set of lattice parameters (a, b, c) is shown in Table 1 of Appendix I.





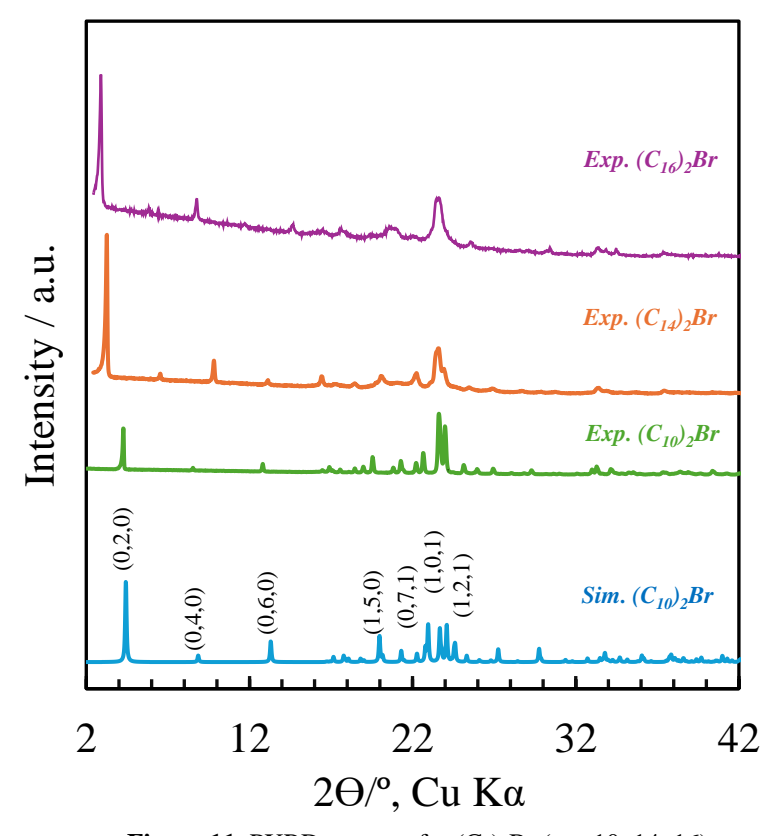


Figure 11. PXRD patterns for $(C_n)_2$ Br (n = 10, 14, 16).

We then plotted the lattice parameter b against the carbon number (n) for $(C_n)_2X$ (X = Cl, Br) (Figure 12). The values are differentiated according to bibliographic data [18] and new data in this project. As the number of carbons in the chain (n) increases, the value of the b-axis increases, following the qualitative assessment of the PXRD patterns. Finally, although the ionic size of bromine cells is larger, the distance between cells is shorter than in chloride-based compounds. Although the ionic radius of bromide (1.95 Å) is larger than that of chloride (1.81 Å), the distances between their cells are shorter. This contradiction is due to the higher polarizability of the Br anion and the geometry of the ammonium confinement plane in crystal structures. In fact, the area of the Br anion plane is large, which favors more efficient molecular packing thanks to stronger dispersive interactions (van der Waals forces) between Br anions and alkyl chains, facilitated by their polarizability. This trade-off between ionic radius and structural organization explains why $(C_n)_2$ Br has shorter intercellular distances than $(C_n)_2$ Cl.





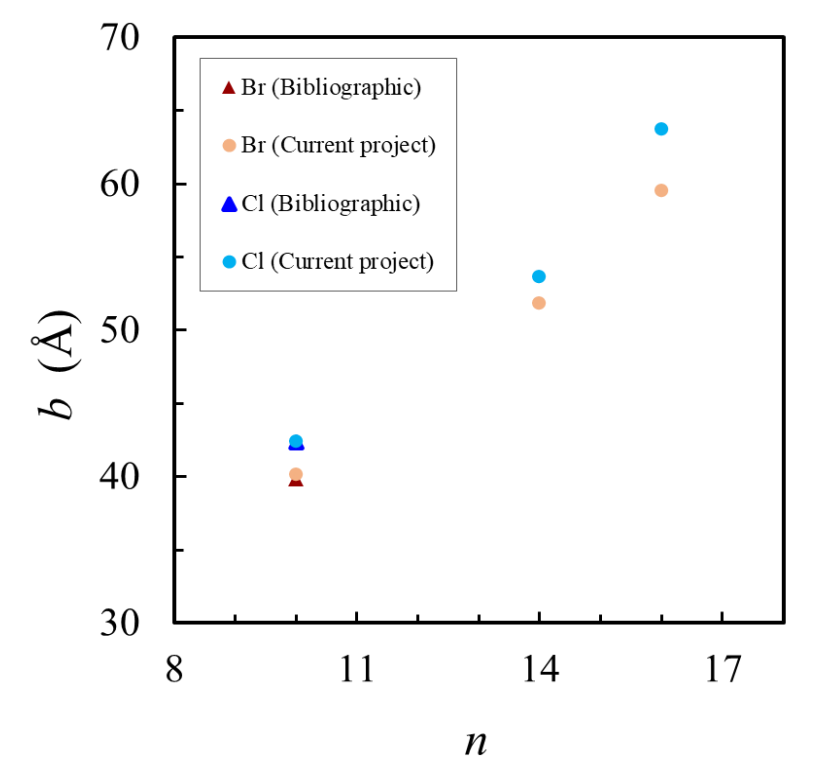


Figure 12. Growth of lattice parameter (b) with respect to the number of carbons in the chain (n).

3.2. THERMODYNAMIC CHARACTERIZATION

This section shows and explains the results of the DSC characterization of $(C_n)_2X$, which were carried out at the *Universitat Politécnica de Catalunya* (UPC) in collaboration with the *Materials Characterization Group* (GCM).

During thermal analysis, a high-enthalpy endothermic transition typically indicates a significant difference in the degree of order between phases. In thermodynamic terms, this transition is characterized by a considerable change in the entropy of the system, a phenomenon typical of processes that transition from a highly ordered phase to a more disordered one. The energy required for this transition is closely related to the intermolecular interactions that stabilize the ordered phase. Thus, when the material is initially in a highly organized phase, a considerable amount of energy (i.e., high latent heat) is required to break these interactions and enable the phase to change. Therefore, quantitative analysis of the enthalpy associated with the transition provides insight into the structural behavior of the material before and after the transition in both endothermic and exothermic processes.

DSCs for $(C_n)_2X$ display a single order-disorder phase transition (Figure 13). Measurements were obtained at different scanning rates (1 K·min⁻¹, 2 K·min⁻¹, 5 K·min⁻¹, 10 K·min⁻¹ and 20 K·min⁻¹), and this slightly influences the result. For higher scanning rates, such as 20 K·min⁻¹, the resolution is lower than for lower scanning rates, such as 1 K·min⁻¹, so the thermal event may not be fully resolved, leading to a less accurate estimation of enthalpy and temperature due to the shorter measurement time. Therefore, a broader peak is obtained, which may prevent the detection of low-energy transitions. Five measurements were conducted in each case to ensure only one transition was detected.





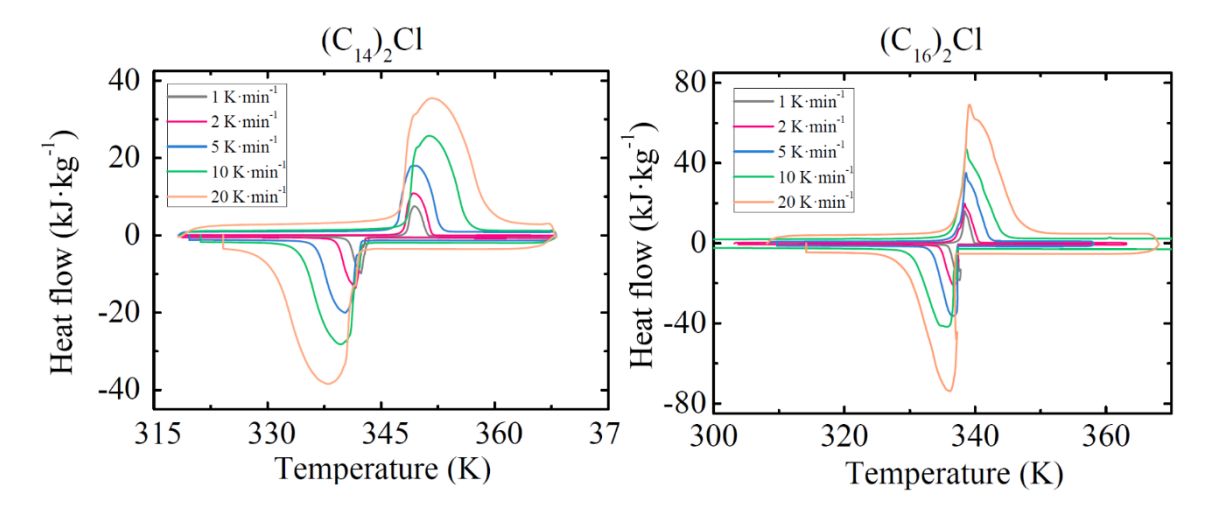


Figure 13. DSC results for $(C_{14})_2Cl$ and $(C_{16})_2Cl$.

Once the compound is heated, the first transition occurs, which consists of going from phase II (lower temperature) to phase I (higher temperature). This transition is endothermic, so heat is absorbed. At the end, as it is a reversible system, it cools down, and another transition occurs, this time exothermic, where heat is released. In this case, the transition occurs from the higher temperature phase (phase I) to the lower temperature phase (phase II). Ideally, the heating (II \rightarrow I) and cooling (I \rightarrow II) processes should occur at the same temperature, as if it were a mirror image; however, it is observed that there is an effect known as hysteresis. Hysteresis is defined as the difference between the thermal profiles during these two processes, and is measured as the difference between the transition temperatures of the heating and cooling stages. For (C_n)₂Cl and (C_n)₂Br (Figure 13), the cooling is shifted towards lower temperatures due to hysteresis, obtaining different behavior in the two states. Therefore, it is very desirable to have a system with minimal hysteresis to improve stability, reduce unnecessary cycling, and then require smaller amounts of external work in practical applications.

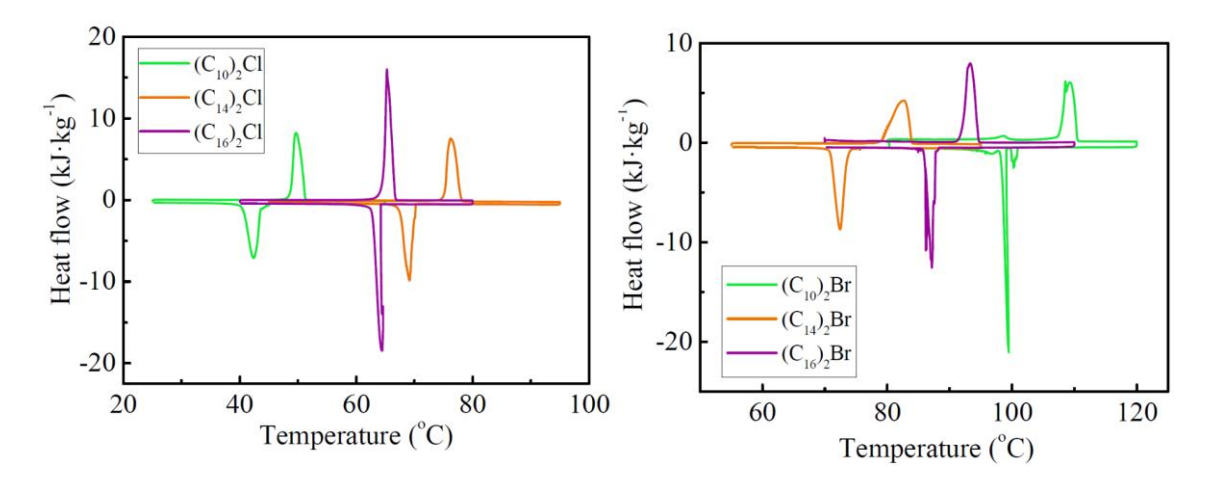


Figure 14. Comparative DSC thermograms of dialkylammonium halide salts with a single reversible transition for each compound (Cl, Br).





In these transitions, the state of aggregation does not change, as they are solid-to-solid. They occur due to a regrouping of the atoms at the molecular level, producing a release/absorption of energy. Analyzing all the results (Figure 14), the most favorable result, both for its low hysteresis ($\Delta T \approx 1$ °C) and for its latent heat and transition temperature values is (C_{16})₂Cl, with a latent heat of 198.2 kJ·kg⁻¹ and a transition temperature of 64.61 °C (Figure 13-14). The second most favorable is (C_{14})₂Cl, since its hysteresis is 6.7 °C, its transition temperature is 75.34 °C, and its latent heat has a value of 138.0 kJ·kg⁻¹ (Figure 13-14).

In the following figures, we present the additional points corresponding to the $(C_n)_2X$ synthesized in this project so that, visually, the improvement in the properties (temperature and latent heat) of the compounds can be observed as the length of the chain (n) increases. The evolution of the *new* $(C_n)_2Cl$ transition temperature and latent heat as a function of chain length was studied (Figure 15). For $(C_n)_2Cl$ (n = 10, 14, and 16), it can be seen that $(C_{10})_2Cl$ has the lowest temperature of all $(48.81 \,^{\circ}\text{C})$, even slightly lower than that of the bibliographic data $(65.05 \,^{\circ}\text{C})$, while the latent heat remains the same $(122.1 \, \text{kJ/kg})$. On the one hand, by analyzing the results for $(C_{14})_2Cl$ and $(C_{16})_2Cl$, which had not yet been studied, it can be seen that $(C_{14})_2Cl$ has a higher transition temperature $(75.34 \,^{\circ}\text{C})$ and latent heat $(138.0 \, \text{kJ/kg})$ than $(C_n)_2Cl$ above $(n \leq 10)$. On the other hand, $(C_{16})_2Cl$ has an exceptionally higher latent heat $(198.2 \, \text{kJ/kg})$ and a lower temperature $(64.61 \,^{\circ}\text{C})$ than $(C_{14})_2Cl$, but still highly favorable.

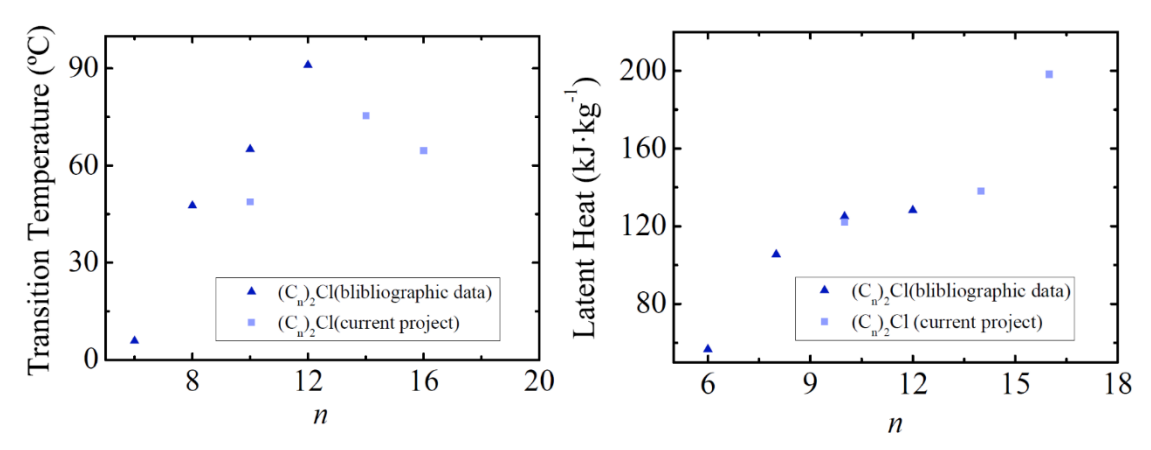


Figure 15. Transition temperature (T_T) and latent heat (ΔH) of $(C_n)_2Cl$ synthesized in the current project (n = 10, 14, 16) graphically compared with those already known (n = 6, 8, 10, 12).

As for $(C_n)_2Br$, values up to n = 18 had been reported, but not for chain lengths of n = 14-16. Therefore, it was decided to synthesize the remaining ones (as well as $(C_{10})_2Br$ as a reference) to evaluate whether the behavior followed the trend already studied. The temperature and latent heat of $(C_{10})_2Br$ (Figure 16) are very similar to those recorded, with a transition temperature of 55.63 °C in both cases, and an experimental latent heat of 111.5 kJ·kg⁻¹, compared to the recorded data $(106.8 \text{ kJ} \cdot \text{kg}^{-1})$. In the case of $(C_{14})_2Br$ and $(C_{16})_2Br$, the transition temperatures increase, reaching 77.90 °C and 92.11 °C, respectively. However, the opposite trend is observed for the latent heat, with values of 130.4 kJ·kg⁻¹ and 123.9 kJ·kg⁻¹. Even so, the results are logical and consistent with previously reported data.





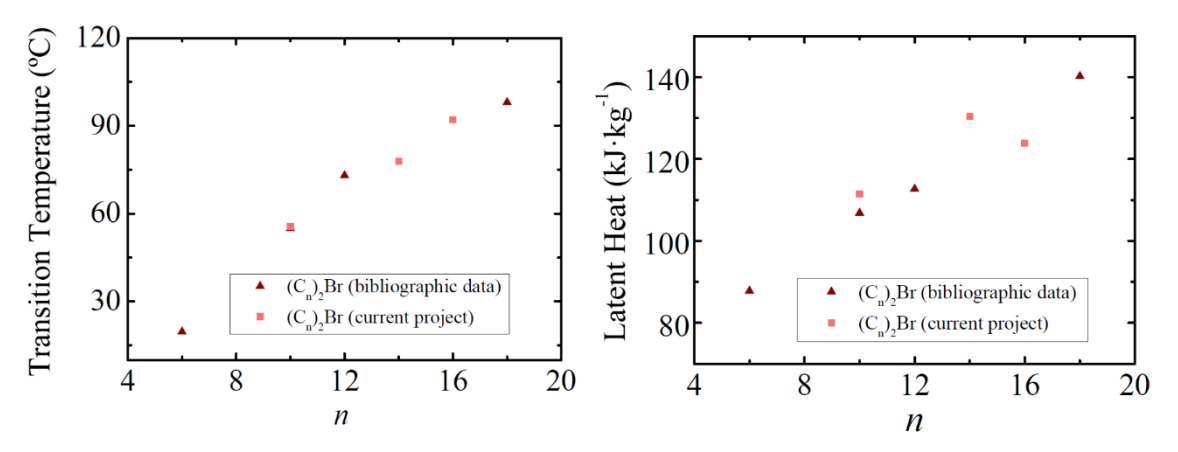


Figure 16. Transition temperature (T_T) and latent heat (ΔH) of $(C_n)_2$ Br synthesized in the current project (n = 10, 14, 16) graphically compared with those already known (n = 6, 10, 12, 18).

3.3. INDUSTRIAL APPLICABILITY OF MATERIALS

Thermal energy storage is emerging as a key strategy to mitigate these losses and improve overall energy efficiency. Although these materials are still emerging and do not have many large-scale implemented applications, from the results, they could be a viable alternative to avoid thermal energy losses due to their high latent heat and thermal stability [27], which translates into high energy density. Industrial heat losses can be produced by conduction, convection, and radiation of products, equipment, and processes, without forgetting the heat released in combustion or steam generation; therefore, it is expected that in the future, they can be implemented in a multitude of systems whose applicability could be extended to industrial sectors working at low-intermediate temperatures (50–90 °C). Some of the applications that are being investigated and are expected to be viable are discussed below.

3.3.1. HEAT PUMPS AND SANITARY HOT WATER

One of the main proposals for the use of these materials is their possible integration into electric heat pump systems or solar thermal panels. This would allow them to store the excess thermal energy generated during the day or during off-peak hours [28], and release it during periods of high energy demand, for example, when fluids need to be heated or preheated.

A conventional heat pump can incorporate encapsulated solid-liquid phase change materials (SL-PCMs), which are typically the most used, but in this case, replacing this system with solid-solid phase change materials would offer numerous advantages over the previous one. The synthesized materials have an operating temperature range of approximately 50 to 100 °C, which could be excellent for conventional heat pump systems (Figure 17) or to produce sanitary hot water (SHW) for industrial and residential applications. Thanks to their solid structure, corrosion and leak problems, typical of current SL-PCMs, would be avoided.





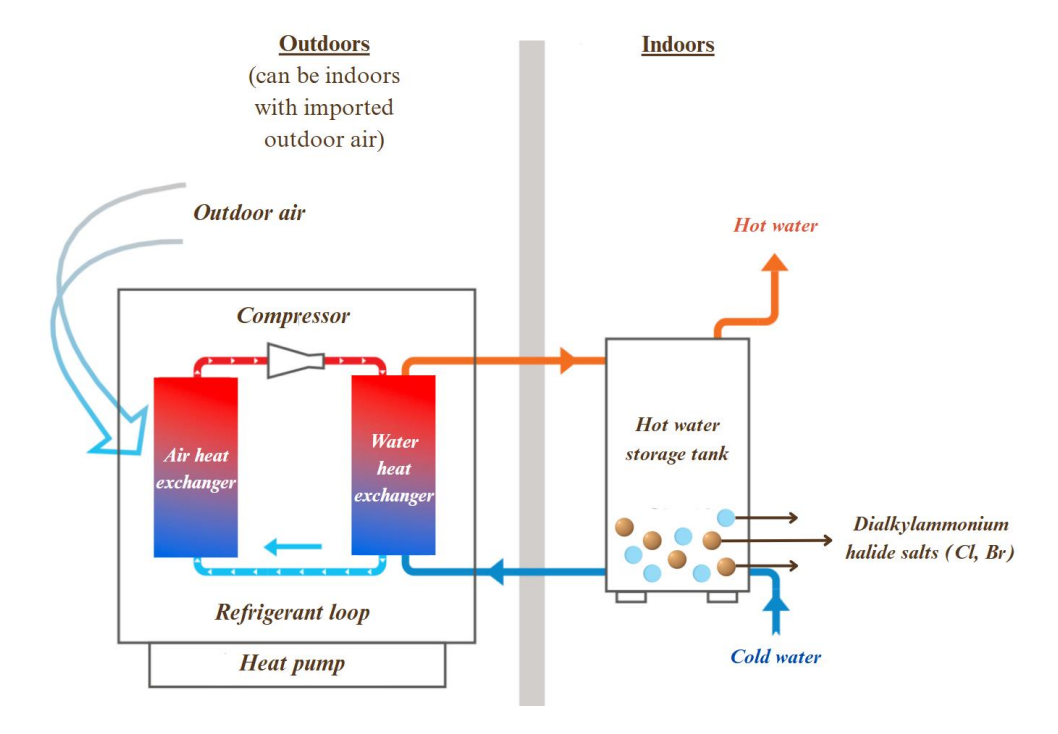


Figure 17. Diagram of a heat pump incorporating a TES system with dialkylammonium halide salts.

In terms of operation, a heat pump typically takes air from outside and compresses it. The heat is transferred to a heat exchanger through which low-temperature water circulates. Through indirect air-water contact, the water reaches a higher temperature and is stored in a nearby tank that would contain the SS-PCMs in compact pellets, granules, or even fixed beds. Once there, the first transition ($\Pi \to I$) would occur, where materials such as dialkylammonium salts would absorb the latent heat of the water and heat up, thus storing their thermal energy. In this transition, the materials would restructure their crystallinity (order-disorder transition) but would not melt or degrade, maintaining the temperature for a while thanks to their high energy density, which would allow them to store more thermal energy in a smaller volume than some SL-PCMs. When hot water was needed, the salts would release the stored heat upon contact with water, producing the next transition ($I \to II$), which would be possible thanks to the reversibility of the process. Moreover, these are non-toxic materials that can significantly reduce energy consumption and heat losses. As a result, the systems are stable and efficient; therefore, they do not usually require excessive maintenance and can operate for several cycles, which gives them a long service life.

3.3.2. BAROCALORIC POTENTIAL

Several studies have shown that dialkylammonium halide salts have a large and reversible barocaloric effect [25], close to room temperature. This effect may be effective in energy-efficient heating and cooling systems. The barocaloric effect occurs when pressure is applied to the material, resulting in temperature changes associated with phase transitions. One of the most promising applications is their use in heat pumps, which represents another avenue other than that discussed above for thermal storage. In this case, solid materials could replace traditional liquid refrigerants, which are typically chemical compounds called hydrofluorocarbons (HCFs). These, when heated, generate greenhouse gases [29] harmful to the environment. If they were replaced by barocaloric materials such as those studied, the system would work by means of a compression-





decompression cycle, where pressure would be applied to the material, releasing heat (the structure would be ordered), and then it would decompress, absorbing heat (the structure would be disordered). An additional advantage of these salts is their low hysteresis during the phase transition, which minimizes energy losses and enhances the reversibility of the cycle. This effect is especially beneficial in repeated compression-decompression operations such as this. This alternative would avoid the use of polluting materials and increase the efficiency of the system.

3.3.3. THERMAL CONTROL IN SUSTAINABLE BUILDING

Another sector that could incorporate these systems is the construction sector. These materials could regulate the thermal sensation of buildings [30] by being integrated into their walls, ceilings, and floors. The installation of structures with these materials could contribute to maintaining more stable interior temperatures, reducing the energy consumption of heating and cooling systems, developing a building construction system, and applying the principle of eco-design. In this way, the system would absorb heat during the day, prevent overheating of interior spaces, and gradually release it during the night, functioning as a system with high thermal inertia.

3.3.4. SYNERGY WITH SOLAR RENEWABLE ENERGY

One of the main proposals for the use of these materials is synergy with renewable energies. In this sector, PCMs play a fundamental role, especially in solar energy systems. This energy presents the problem of intermittency and fluctuating availability due to diurnal and seasonal meteorological changes. Therefore, it is considered that the materials developed could solve this obstacle, storing thermal energy during the hours of high production to supply it at night or during hours of low solar activity. This solution would provide reliability and continuity to the system, with a strong commitment to renewable energies. In this regard, these materials are intended for use in systems with operating temperature ranges of approximately 50–100 °C, which could include private, domestic, or low-temperature industrial applications.

3.3.5. INTEGRATION OF SS-PCMs INTO BATTERY DESIGN

The integration of PCMs in battery design could prove to be highly efficient and solve problems commonly encountered in these systems. These materials could absorb excess heat generated by intense discharges or during fast charges [31], as the system tends to overheat. During the phase change, the PCM would act by absorbing large amounts of thermal energy without significantly increasing the temperature.

This integration would keep the battery operation safe, increasing its reliability and also preventing thermal propagation, which would help to avoid fires. PCMs appear to be a more efficient alternative to current liquid cooling systems, as they would not require auxiliary equipment such as pumps or fans. They would also be better than air-cooled systems, as they would offer a larger contact surface and direct contact with the cells.

These materials, due to their adequate thermal and chemical stability, could reduce energy consumption and eliminate risks associated with overheating. On the other hand, their cost could be higher compared to the conventional systems mentioned above.





4. Experimental methods

4.1. MATERIALS

4.1.1. REAGENTS

The chemicals used in the different syntheses were didecylamine (98%, BLD pharm), ditetradecylamine (95%, BLD pharm), dihexadecylamine (98%, BLD pharm), hydrochloric acid (37%, Sigma-Aldrich), hydrobromic acid (48%, Sigma-Aldrich), and hexane (≥97%, Sigma-Aldrich). All at room temperature.

4.1.2. SYNTHESIS OF $(C_n)_2Cl$

4.1.2.1. SYNTHESIS OF (C₁₀H₂₁)₂NH₂Cl

For the synthesis of $(C_{10})_2Cl$, 297.56 mg (1 mmol, 1 eq.) of didecylamine $(C_{10})_2$ (98% purity) was dissolved in 1.10 mL of hexane while stirring at room temperature. To this solution, 99 μ L of HCl (37 wt. %) (1.2 mmol, 1.2 eq.) was added dropwise while stirring. After adding hydrochloric acid, a white mass immediately began forming in the solution. The reaction mixture was stirred for 2 hours to complete the reaction. Once the reaction was complete, it was found that a whitish compound had formed. The precipitate was filtered and washed twice with hexane (2 x 10 mL), and then with distilled water (2 x 10 mL), obtaining a white compact powder. Finally, the sample was dried under vacuum for 12 h to obtain white powder.

4.1.2.2. SYNTHESIS OF (C14H29)2NH2Cl

For the synthesis of $(C_{14})_2Cl$, 204.50 mg (0.5 mmol, 1 eq.) of ditetradecylamine $(C_{14})_2$ (95% purity) was dissolved in 2.55 mL of hexane while stirring at room temperature. To this solution, 50 μ L of HCl (37 wt. %) (0.6 mmol, 1.2 eq.) was added dropwise while stirring. After adding hydrochloric acid, a white mass immediately began forming in the solution. The reaction mixture was stirred for 2 hours to complete the reaction. Once the reaction was complete, it was found that a whitish compound had formed. The precipitate was filtered, washed twice with hexane (2 x 10 mL), and then twice with distilled water (2 x 10 mL), obtaining a white compact powder. Finally, the sample was dried under vacuum for 12 h to obtain white powder.

4.1.2.3. SYNTHESIS OF (C₁₆H₃₃)₂NH₂Cl

For the synthesis of $(C_{16})_2Cl$, 93.50 mg (0.2 mmol, 1 eq.) of dihexadecylamine $(C_{16})_2$ (98% purity) was dissolved in 2.20 mL of hexane while stirring at room temperature. To this solution, 20 μ L of HCl (37 wt. %) (0.24 mmol, 1.2 eq.) was added dropwise while stirring. After adding hydrochloric acid, a white mass immediately began forming in the solution. The reaction mixture was stirred for 2 hours to complete the reaction. Once the reaction was complete, it was found that a whitish compound had formed. The precipitate was filtered, then washed twice with hexane (2 x 10 mL). In this case, it was not washed with distilled water since it was observed that, for compounds with longer alkyl chains, particularly in the case of $(C_{16})_2Cl$, the molecule becomes more hydrophobic. This reduces its affinity with water and the effectiveness of the washing process. A compact white powder was obtained. Finally, the sample was vacuum-dried for 12 h to obtain white powder.





4.1.3. SYNTHESIS OF $(C_n)_2$ Br

4.1.3.1. SYNTHESIS OF (C₁₀H₂₁)₂NH₂Br

For the synthesis of $(C_{10})_2$ Br, 296.30 mg (1 mmol, 1 eq.) of didecylamine $(C_{10})_2$ (98% purity) was dissolved in 1.10 mL of hexane while stirring at room temperature. To this solution, 136 μ L of HBr (48 wt. %) (1.2 mmol, 1.2 eq.) was added dropwise while stirring. After adding hydrobromic acid, a white mass immediately began forming in the solution. The reaction mixture was stirred for 2 hours to complete the reaction. Once the reaction was complete, it was found that a whitish compound had formed. The precipitate was filtered, washed twice with hexane (2 x 10 mL), and then twice with distilled water (2 x 10 mL), obtaining a white compact powder. Finally, the sample was dried under vacuum for 12 h to obtain white powder.

4.1.3.2. SYNTHESIS OF (C₁₄H₂₉)₂NH₂Br

For the synthesis of $(C_{14})_2Br$, 204.20 mg (0.5 mmol, 1 eq.) of ditetradecylamine $(C_{14})_2$ (95% purity) was dissolved in 2.55 mL of hexane while stirring at room temperature. To this solution, 68 μ L of HBr (48 wt. %) (0.6 mmol, 1.2 eq.) was added dropwise while stirring. After adding hydrobromic acid, a white mass immediately began forming in the solution. The reaction mixture was stirred for 2 hours to complete the reaction. Once the reaction was complete, it was found that a whitish compound had formed. The precipitate was filtered, washed twice with hexane (2 x 10 mL), and then twice with distilled water (2 x 10 mL), obtaining a white compact powder. Finally, the sample was dried under vacuum for 12 h to obtain white powder.

4.1.3.3. SYNTHESIS OF (C₁₆H₃₃)₂NH₂Br

For the synthesis of $(C_{16})_2Br$, 93.20 mg (0.2 mmol, 1 eq.) of dihexadecylamine $(C_{16})_2$ (98% purity) was dissolved in 2.20 mL of hexane while stirring at room temperature. To this solution, 27 μ L of HBr (48 wt. %) (0.24 mmol, 1.2 eq.) was added dropwise while stirring. After adding hydrobromic acid, a white mass immediately began forming in the solution. The reaction mixture was stirred for 2 hours to complete the reaction. Once the reaction was complete, it was found that a whitish compound had formed. The precipitate was filtered, then washed twice with hexane (2 x 10 mL). In this case, it was not washed with distilled water since it was observed that, for compounds with longer alkyl chains, the molecule becomes more hydrophobic. This reduces its affinity with water and the effectiveness of the washing process. A compact white powder was obtained. Finally, the sample was vacuum-dried for 12 h to obtain white powder.

4.2. METHODS

4.2.1. POWDER X-RAY DIFFRACTION (PXRD)

Each of the samples to be analyzed were compacted between 3.6 microns of thick polyester *mylar* films and measured in a *PANalytical X'Pert PRO MPD* θ/θ 240-millimeter radius powder diffractometer in convergent beam configuration with focusing mirror and transmission geometry with flat samples sandwiched between low absorption films. The values set are a radiation Cu K α (α = 1.5418 Å) and a working power of 45 kV-40 mA. The incident beam slits have a height of 0.4 millimeters. *Soller* slits are 0.02 radians for the incident and diffracted beam. In addition, there is a *PIXcel* detector whose active length is 3.347 °. The 2 θ/θ scans from 2 to 60 °2 θ , with a step size of 0.026 °2 θ , and a measuring time of 300 seconds per step.





4.2.2. BALL MILLING

Powders of each dialkylammonium halide salt are added to a 2 ml Eppendorf vial and milled at room temperature using a 3 mm zirconium ball for 30 minutes at 30 Hz in a Retsch MM400 mill.

4.2.3. DIFFERENTIAL SCANNING CALORIMETRY (DSC)

Differential scanning calorimetry (DSC) at atmospheric pressure was performed at the *Universitat Politécnica de Catalunya* (UPC), thanks to the *Materials Characterization Group* (GCM), using a Q100 DSC from TA Instruments. The samples were hermetically encapsulated in an aluminum capsule. The sample volume was between 5.5 and 7.0 mg. The analysis measured temperature variation and heat flux. The heating and cooling rates were 1 K·min⁻¹, 2 K·min⁻¹, 5 K·min⁻¹, 10 K·min⁻¹ and 20 K·min⁻¹.





5. Conclusions

Finally, after the successful synthesis and characterization of new dialkylammonium halide salts, with two different halides (Cl and Br) and different alkyl chain lengths (n = 10, 14, 16), it can be stated that these materials exhibit a unique reversible solid-solid phase transition during heating and cooling processes. This transition corresponds with a high latent heat, which allows these compounds to store and release large amounts of thermal energy without undergoing a phase change to a liquid or gas state. The results reveal a clear trend of increasing latent heat, and in most cases transition temperature, as the alkyl chain length increases.

After analysis of the PXRD patterns, the growth of the lattice parameter b as the chain length increases was confirmed, demonstrating the direct influence of the molecular structure on the crystalline organization. In fact, it confirmed a balance between ionic radius and structural organization, which explains why $(C_n)_2$ Br presents shorter intercellular distances than $(C_n)_2$ Cl, even though the bromide has a larger ionic size.

Based on the results obtained, it is important to highlight that $(C_n)_2Cl$ compounds are more favorable than $(C_n)_2Br$, since they show a higher overall performance as SS-PCMs. This is because they possess higher latent heats and lower hysteresis values, which reduces the need for additional energy input during thermal loading and unloading cycles in future applications. In addition, $(C_n)_2Cl$ materials have transition temperatures that are in suitable ranges for industrial heat recovery applications. On the other hand, $(C_n)_2Br$ materials, such as $(C_{16})_2Br$ stand out mainly for having a higher transition temperature $(92.11 \, ^{\circ}C)$ with medium-high latent heat values $(123.9 \, \text{kJ} \cdot \text{kg}^{-1})$. Undoubtedly, the most promising result is compound $(C_{16})_2Cl$, with a latent heat of 198.2 kJ·kg⁻¹and a transition temperature of 64.61 $^{\circ}C$, not to mention its reduced hysteresis value $(\Delta T \approx 1 \, ^{\circ}C)$.

Compared to previously studied 2D perovskite-based PCMs, these dialkylammonium halide salts exhibit similar transition temperatures; however, the latent heat values are higher. Moreover, their metal-free nature, synthetic accessibility, and thermal reversibility make them promising candidates for sustainable thermal energy storage systems. In summary, this work extends the family of solid-solid phase change materials and opens new perspectives for their integration into technologies such as heat pumps, solar thermal storage, thermoregulation, solar PV, and solar photovoltaics. On the other hand, these materials can be synthesized from more accessible raw materials and could be more economical due to the absence of metals in their structure.

Developing these materials at this temperature range could contribute to a more sustainable energy transition, adding value to industrial waste heat, improving the energy efficiency of current industrial processes, and reducing dependence on fossil fuels by integrating these materials into renewable energy systems. These materials could be implemented in heat pump systems, battery design, and sustainable construction, among other applications mentioned in the report. Given these promising results, further study of these materials could be proposed, increasing the chain length to obtain PCM with even higher temperatures and latent heat.





6. References

- [1] Forman, C., Kolawole Muritala, I., Pardemann, R., & Meyer, B. (2015, October 27). *Estimating the global waste heat potential*. ScienceDirect. http://dx.doi.org/10.1016/j.rser.2015.12.192
- ^[2] Lloveras, P. (Ed.). (2023). Barocaloric Effects in the Solid State: Materials and Methods. Chapter 1: Introduction to the barocaloric effect and Chapter 6: Hybrid organic—inorganic materials: introducing soft barocaloric materials for low-pressure applications. Institute of Physics Publishing. 10.1088/978-0-7503-4690-0
- [3] Fallahi, A., Guldentops, G., Tao, M., Granados-Focil, S., & Van Dessel, S. (2017, August 25). *Review on solid-solid phase change materials for thermal energy storage: Molecular structure and thermal properties.* ScienceDirect. http://dx.doi.org/10.1016/j.applthermaleng.2017.08.161
- ^[4] Zhi, M., Yue, S., Zheng, L., Su, B., Fu, J., & Sun, Q. (2024). *Recent developments in solid-solid phase change materials for thermal energy storage applications*. Journal of Energy Storage, 89, 111570. https://doi.org/10.1016/J.EST.2024.111570
- [5] Chen, X., Gao, H., Tang, Z., & Wang, G. (2020). *Metal-Organic Framework-based Phase Change Materials for Thermal Energy Storage*. Cell Reports Physical Science, *1*(10). https://doi.org/10.1016/j.xcrp.2020.100218
- ^[6] Wu, B., Wang, Y., Liu, Z., Liu, Y., Fu, X., Kong, W., Jiang, L., Yuan, Y., Zhang, X., & Lei, J. (2019). *Thermally reliable, recyclable and malleable solid-solid phase-change materials through the classical Diels-Alder reaction for sustainable thermal energy storage*. Journal of Materials Chemistry A, 7(38), 21802-21811. https://doi.org/10.1039/C9TA08368E
- [7] A. Usman, F. Xiong, W. Aftab, M. Qin, R. Zou, *Emerging Solid-to-Solid Phase-Change Materials for Thermal-Energy Harvesting*, *Storage*, and *Utilization*. Adv. Mater. 2022, 34, 2202457. https://doi.org/10.1002/adma.202202457
- [8] Ben, J. G., María, P., Señarís Rodríguez, A., Manuel, J., & García, B. (2024). *Innovative materials chemistry strategies for engineered-enhanced thermomaterials for barocaloric and related solid-state refrigeration*. Lenguas Modernas, 62, Chapter 3, page 47. http://hdl.handle.net/2183/34595
- ^[9] Hong, H., Guo, S., Jin, L., Mao, Y., Chen, Y., Gu, J., Chen, S., Huang, X., Guan, Y., Li, X., Li, Y., Lü, X., & Fu, Y. (2024). *Two-dimensional lead halide perovskite lateral homojunctions enabled by phase pinning*. Nature Communications 2024 15:1, 15(1), 1–9. https://doi.org/10.1038/s41467-024-47406-1
- [10] Li, S., He, L., Lu, H., Hao, J., Wang, D., Shen, F., Song, C., Liu, G., Du, P., Wang, Y., & Cong, D. (2023). *Ultrahigh-performance solid-solid phase change material for efficient, high-temperature thermal energy storage*. Acta Materialia, 249, 118852. https://doi.org/10.1016/J.ACTAMAT.2023.118852
- [11] Li, J., Barrio, M., Dunstan, D. J., Dixey, R., Lou, X., Tamarit, J.-L., Phillips, A. E., Lloveras, P., Li, J., Dunstan, D. J., Dixey, R., Phillips, A. E., Lou, X., Barrio, M., Tamarit, J.-L., & Lloveras, P. (2021). Colossal Reversible Barocaloric Effects in Layered Hybrid Perovskite (C10H21NH3)2MnCl4 under Low Pressure Near Room Temperature. Advanced Functional Materials, 31(46), 2105154. https://doi.org/10.1002/ADFM.202105154





- [12] Venkitaraj, K. P., Praveen, B., Singh, H., & Suresh, S. (2020). Low melt alloy blended polyalcohol as solid-solid phase change material for energy storage: An experimental study. Applied Thermal Engineering, 175, 115362. https://doi.org/10.1016/J.APPLTHERMALENG.2020.115362
- [13] Kahwaji, Samer & White, Mary. (2021). Organic Phase Change Materials for Thermal Energy Storage: Influence of Molecular Structure on Properties. Molecules. 26. 6635. https://doi.org/10.3390/molecules26216635
- [14] Huang, J., Weng, M., Yu, J., Sun, L., Zeng, H., Liu, Y., Zeng, W., Min, Y., & Guo, Z. (2021). *Advances and Applications of Phase Change Materials (PCMs) and PCMs-based Technologies*. ES Materials and Manufacturing, *13*, 23-39. https://doi.org/10.30919/ESMM5F458
- [15] Bayon, A., Liu, M., Sergeev, D., Grigore, M., Bruno, F., & Müller, M. (2019). *Novel solid-solid phase-change cascade systems for high-temperature thermal energy storage*. Solar Energy, 177, 274-283. https://doi.org/10.1016/J.SOLENER.2018.10.085
- ^[16] Cheng, T., Wang, N., Wang, H., Sun, R., & Wong, C. P. (2020). *A newly designed paraffin@VO2 phase change material with the combination of high latent heat and large thermal conductivity*. Journal of Colloid and Interface Science, 559, 226-235. https://doi.org/10.1016/J.JCIS.2019.10.033
- ^[17] Junaid, M. F., Rehman, Z. ur, Čekon, M., Čurpek, J., Farooq, R., Cui, H., & Khan, I. (2021). *Inorganic phase change materials in thermal energy storage: A review on perspectives and technological advances in building applications*. Energy and Buildings, 252, 111443. https://doi.org/10.1016/J.ENBUILD.2021.111443
- [18] Steinert, S., Voigt, W., Glausch, R., & Neuschütz, M. (2005). *Thermal characteristics of solid-solid phase transitions in long-chain dialkylammonium salts*. Thermochimica Acta, 435(1), 28-33. https://doi.org/10.1016/J.TCA.2005.04.019
- [19] Jinnouchi, R., Lahnsteiner, J., Karsai, F., Kresse, G., & Bokdam, M. (2019). *Phase Transitions of Hybrid Perovskites Simulated by Machine-Learning Force Fields Trained on the Fly with Bayesian Inference*. Physical Review Letters, *122*(22), 225701. https://doi.org/10.1103/PhysRevLett.122.225701
- [20] Thakur, D., & Chang, S. H. (2024). *Material properties and optoelectronic applications of lead halide perovskite thin films*. Synthetic Metals, *301*, 117535. https://doi.org/10.1016/j.synthmet.2023.117535
- [21] Quan, L. N., García de Arquer, F. P., Sabatini, R. P., & Sargent, E. H. (2018). *Perovskites for Light Emission*. Advanced Materials, 30(45). https://doi.org/10.1002/ADMA.201801996
- [22] Escorihuela-Sayalero, C., Sanuy, A., Pardo, L. C., & Cazorla, C. (2024). *Orientational disorder and molecular correlations in hybrid organic-inorganic perovskites: From fundamental insights to technological applications*. https://arxiv.org/pdf/2407.20672
- ^[23] Seo, J., McGillicuddy, R. D., Slavney, A. H., Zhang, S., Ukani, R., Yakovenko, A. A., Zheng, S. L., & Mason, J. A. (2022). *Colossal barocaloric effects with ultralow hysteresis in two-dimensional metal-halide perovskites*. Nature Communications 2022 13:1, 13(1), 1-15. https://doi.org/10.1038/S41467-022-29800-9
- [24] Ribas Cabello, L. (2025). *Two-dimensional copper perovskites for barocaloric devices operating circa 100 °C*. Final Degree Works Chemistry. https://diposit.ub.edu/dspace/handle/2445/219403

Developing dialkylammonium halide salts for industrial heat recovery at medium temperatures



- [25] Jinyoung Seo, Rahil Ukani, Juanjuan Zheng, Jason D. Braun, Sicheng Wang, Faith E. Chen, Hong Ki Kim, Selena Zhang, Catherine Thai, Ryan D. McGillicuddy, Hao Yan, Joost J. Vlassak, and Jarad A. Mason. *Barocaloric Effects in Dialkylammonium Halide Salts*. Journal of the American Chemical Society **2024** *146* (4), 2736-2747. https://pubs.acs.org/doi/10.1021/jacs.3c12402
- [26] Matuszek, K., Kar, M., Pringle, J. M., & Macfarlane, D. R. (2023). *Phase Change Materials for Renewable Energy Storage at Intermediate Temperatures*. Chemical Reviews, 123(1), 491–514. https://pubs-acs-org.sire.ub.edu/doi/10.1021/acs.chemrev.2c00407
- ^[27]Lopez-Morales, J. L., Perez-Arce, J., Serrano, A., Dauvergne, J. L., Casado, N., Kottarathil, A., Palomo Del Barrio, E., & Garcia-Suarez, E. J. (2023). *Protic dialkylammonium-based ionic liquids as promising solid-solid phase change materials for thermal energy storage: Synthesis and thermo-physical characterization*. Journal of Energy Storage, 72, 108379. https://doi.org/10.1016/J.EST.2023.108379
- ^[28]Ram M, Bogdanov D, Aghahosseini A, Gulagi A, Oyewo AS, Child M, Caldera U, Sadovskaia K, Farfan J, Barbosa L, Fasihi M, Khalili S, Fell H-J, Breyer C, Global Energy System based on 100% Renewable Energy *Energy Transition in Europe Across Power, Heat, Transport and Desalination Sectors*, LUT University and Energy Watch Group, Lappeenranta, Berlin (2018). (27). ISBN: 978-952-335-329-9
- ^[29] Velders, G. J. M., Daniel, J. S., Montzka, S. A., Vimont, I., Rigby, M., Krummel, P. B., Muhle, J., O'Doherty, S., Prinn, R. G., Weiss, R. F., & Young, D. (2022). *Projections of hydrofluorocarbon (HFC) emissions and the resulting global warming based on recent trends in observed abundances and current policies*. Atmospheric Chemistry and Physics, 22(9), 6087–6101. https://doi.org/10.5194/ACP-22-6087-2022
- [30] Jha, S. K., Sankar, A., Zhou, Y., & Ghosh, A. (2024). *Incorporation of Phase Change Materials in Buildings*. Construction Materials 2024, Vol. 4, Pages 676-703, 4(4). https://doi.org/10.3390/CONSTRMATER4040037
- e-Mobility Engineering. (2025). *Phase Change Materials for EV Battery Thermal Management*. https://www.emobility-engineering.com/phase-change-materials-ev-battery-thermal-management/





7. ACRONYMS

- 2D: Two-dimensional
- 3D: Three-dimensional
- $(C_{10})_2$: $[CH_3(CH_2)_9]_2NH$ (Didecylamine)
- (C₁₄)₂ [CH₃(CH₂)₁₃]₂NH (Ditetradecylamine)
- (C₁₆)₂: [CH₃(CH₂)₁₅]₂NH (Dihexadecylamine)
- (C₁₀)₂Cl: (C₁₀H₂₁)₂NH₂Cl (*N*,*N*-didecylammonium chloride)
- (C₁₄)₂Cl: (C₁₄H₂₉)₂NH₂Cl (N,N-dithretradecylammonium chloride)
- (C₁₆)₂Cl: (C₁₆H₃₃)₂NH₂Cl (N,N-dihexadecylammonium chloride)
- $(C_{10})_2$ Br: $(C_{10}H_{21})_2$ NH₂Br $(N,N-didecylammonium\ bromide)$
- $(C_{14})_2$ Br: $(C_{14}H_{29})_2$ NH₂Br (N,N-dithret rade cylammonium bromide)
- (C₁₆)₂Br: (C₁₆H₃₃)₂NH₂Br (N,N-dihexadecylammonium bromide)
- DSC: Differential Scanning Calorimetry
- HCFs: Hydrofluorocarbons
- PCMs: Phase Change Materials
- PXRD: Powder X-Ray Diffraction
- SCXRD: Single Crystal X-Ray Diffraction
- **SHW**: Sanitary Hot Water
- **SL-PCMs**: Solid-Liquid Phase Change Materials
- **SS-PCMs**: Solid-Solid Phase Change Materials
- TES: Thermal Energy Storage





APPENDICES





APPENDIX I. PXRD DATA

Table 1. Results of the lattice parameters a, b, c (Å) for each simulated and experimental sample $(\lambda = 1.54054 \text{ Å}).$

Sample	а	b	c
Simulated (C ₁₀) ₂ Cl	4.82	42.319	5.29
Experimental (C ₁₀) ₂ Cl	4.84	42.410	5.29
Experimental (C ₁₄) ₂ Cl	4.65	53.625	5.29
Experimental (C ₁₆) ₂ Cl	4.65	63.714	5.40
Simulated (C ₁₀) ₂ Br	5.35	39.862	5.28
Experimental (C ₁₀) ₂ Br	5.36	40.152	5.50
Experimental (C ₁₄) ₂ Br	5.35	51.833	5.29
Experimental (C ₁₆) ₂ Br	5.35	59.542	5.25





APPENDIX II. DSC DATA

Table 2. Numerical results of transition temperature and latent heat values extracted by DSC for each synthesized powder.

	Scanning Heating		Cooling		
Sample	rate (K·min ⁻¹)	Tonset (°C)	Latent Heat (kJ·kg ⁻¹)	Tonset (°C)	Latent Heat (kJ·kg ⁻¹)
	1	48.81	122.1	43.56	-125.8
	2	48.74	121.8	43.20	-125.1
$(C_{10})_2Cl$	5	48.94	119.4	43.24	-120.1
	10	48.83	118.4	43.01	-118.9
	20	48.89	120.7	42.67	-119.5
	1	55.49	107.4	52.07	-110.5
	2	55.44	107.1	52.02	-110.3
$(C_{10})_2Br$	5	55.64	109.0	50.80	-109.3
	10	55.47	109.2	51.72	-111.0
	20	55.63	111.5	51.58	-112.1
	1	75.23	133.3	69.83	-142.0
	2	74.83	132.8	69.47	-140.7
$(C_{14})_2Cl$	5	73.95	133.8	68.69	-139.3
	10	75.34	138.0	68.65	-137.1
	20	74.45	136.1	68.08	-134.6
(C ₁₄) ₂ Br	1	79.12	122.6	73.57	-132.7
	2	78.92	121.1	72.48	-129.8
	5	78.82	128.1	73.59	-130.4
	10	78.21	129.9	73.40	-131.3
	20	77.90	130.4	73.24	-129.1
	1	64.75	196.6	-	-197.9
(C ₁₆) ₂ Cl	2	64.46	187.8	64.21	-194.1
	5	64.55	194.8	64.26	-197.7
	10	64.19	194.7	63.57	-187.7
	20	64.61	198.2	-	-200.4
	1	92.11	123.9	87.37	-118.2
	2	92.25	114.7	97.30	-114.2
$(C_{16})_2Br$	5	92.06	110.9	86.86	-112.4
	10	92.00	111.0	86.45	-112.6
	20	92.06	109.3	86.22	-106.6





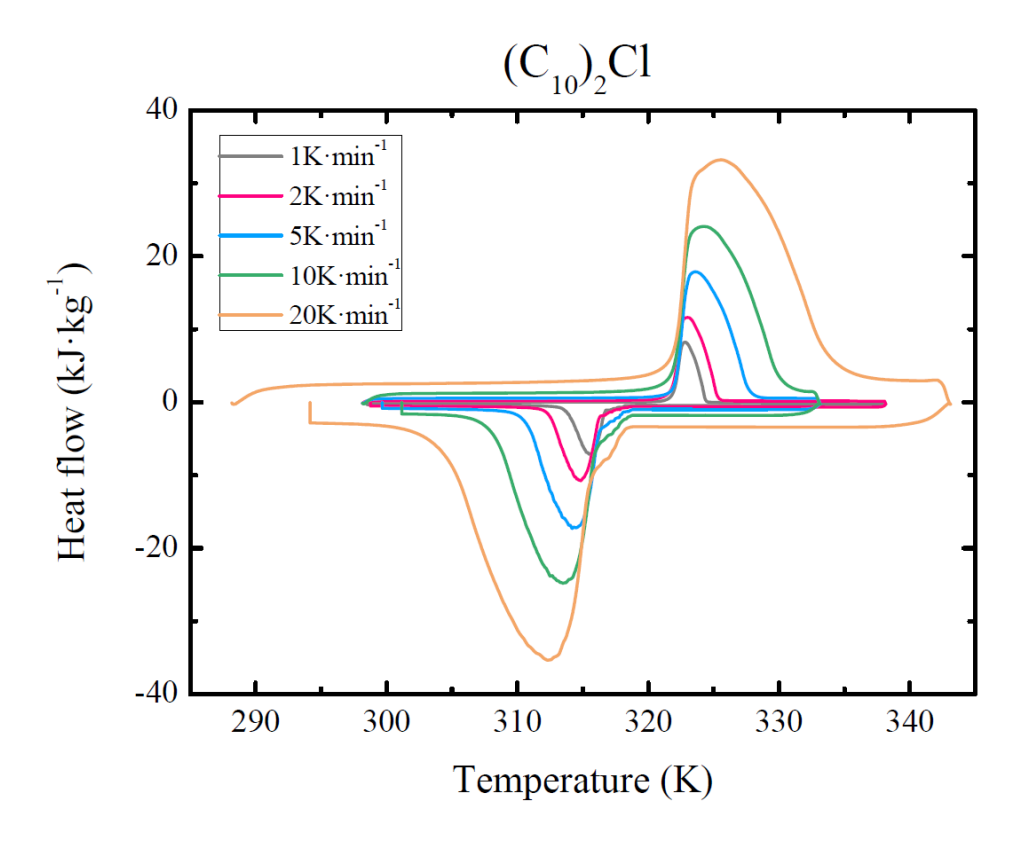


Figure 18. DSC results for $(C_{10})_2Cl$.

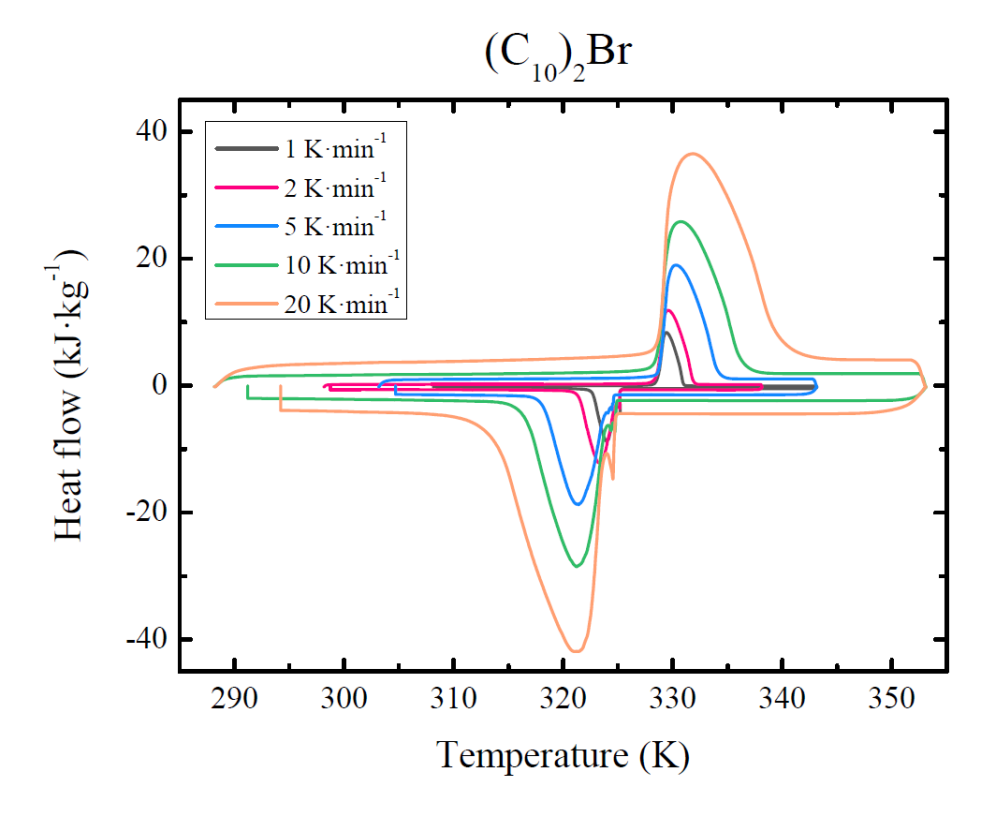


Figure 19. DSC results for $(C_{10})_2Br$.





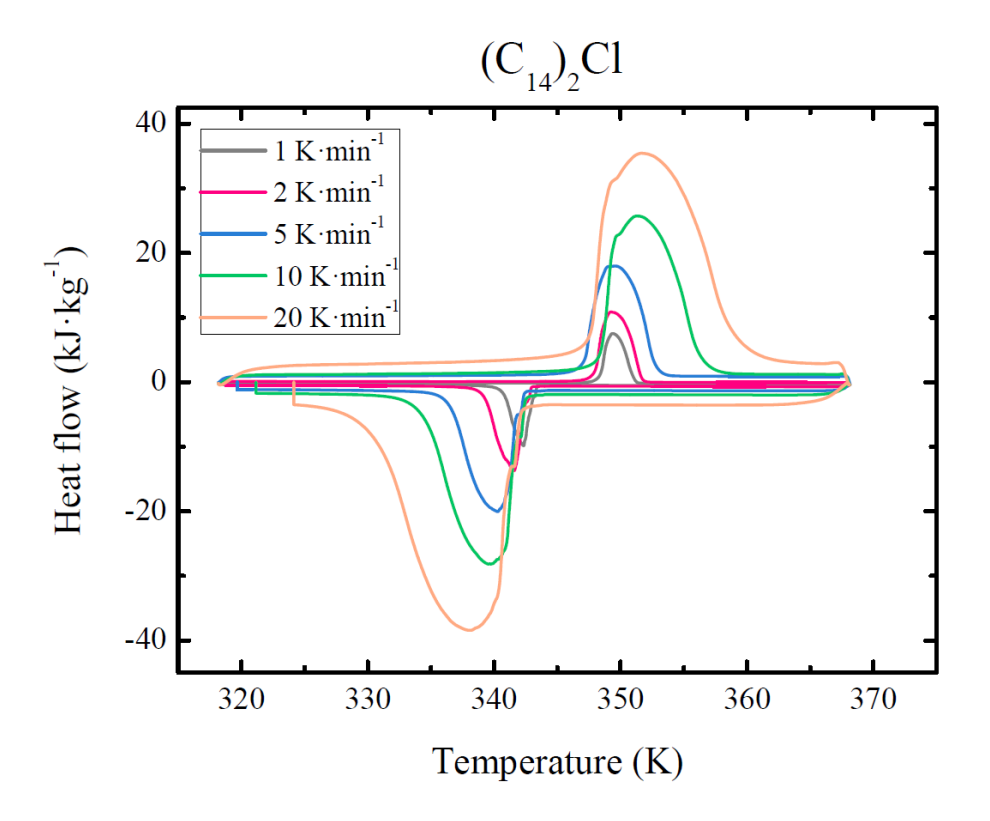


Figure 20. DSC results for $(C_{14})_2Cl$.

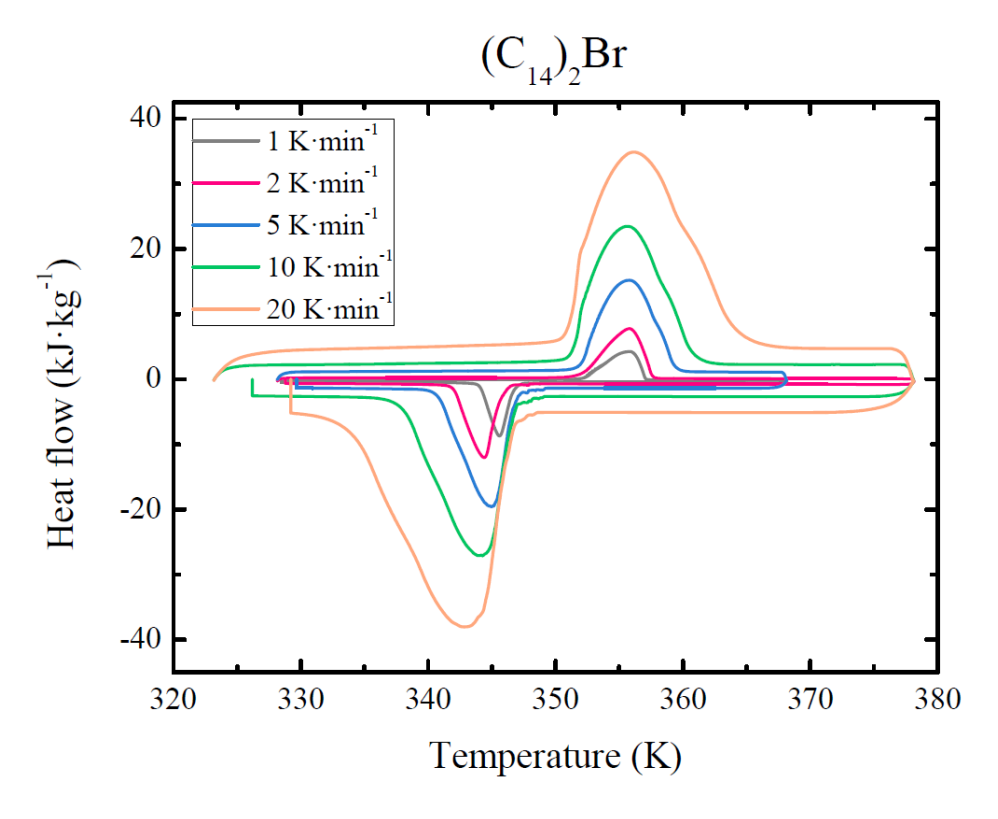


Figure 21. DSC results for $(C_{14})_2$ Br.





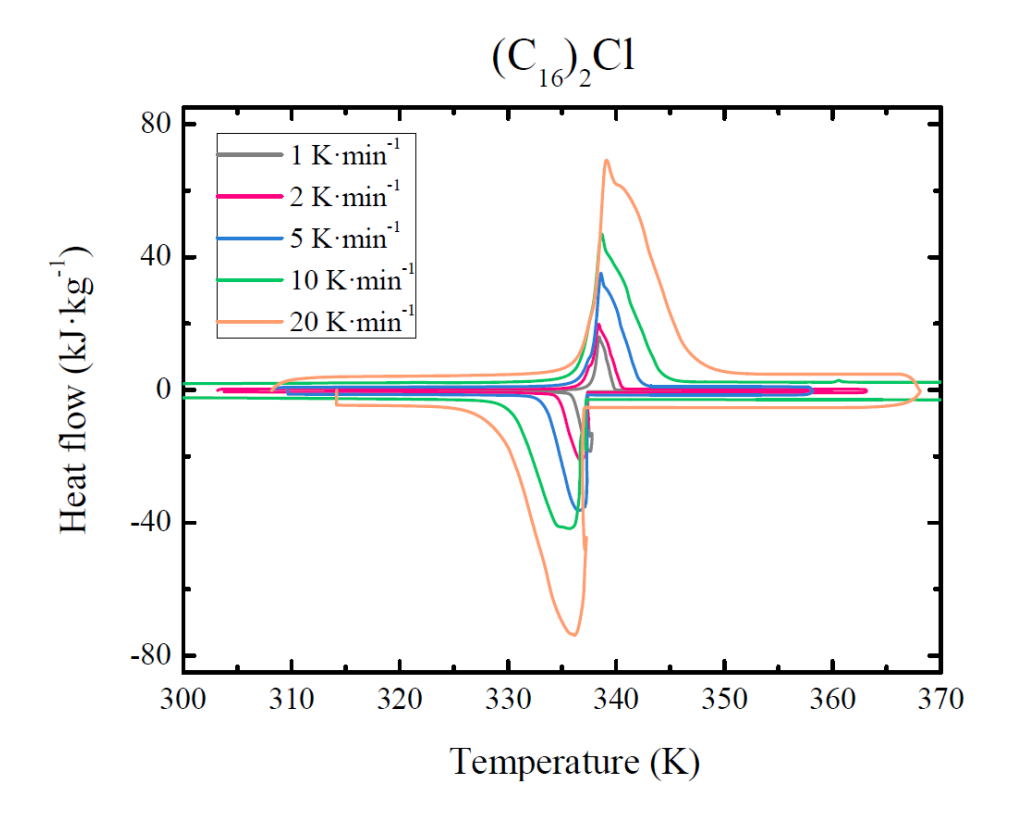


Figure 22. DSC results for $(C_{16})_2Cl$.

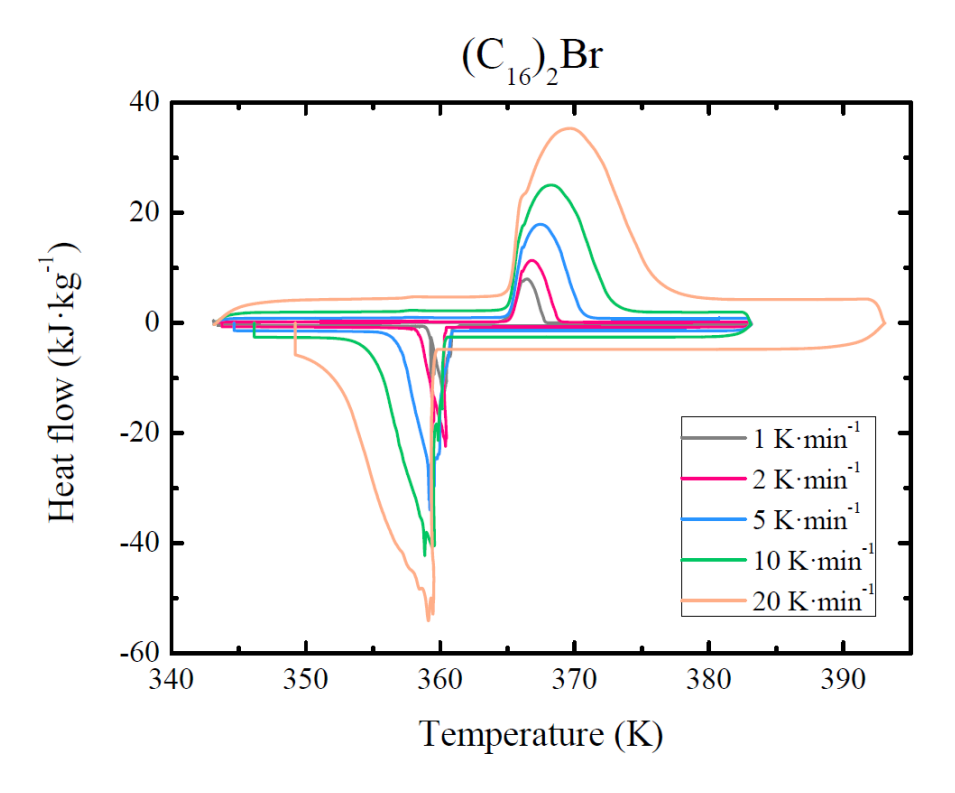


Figure 23. DSC results for $(C_{16})_2$ Br.